DEVELOPMENT OF PLASMA ACTUATORS FOR HIGH-SPEED FLOW CONTROL BASED ON NANOSECOND REPETITIVELY PULSED DIELECTRIC BARRIER DISCHARGES

by

Aarthi Devarajan

A Thesis

Submitted to the Faculty of Purdue University

In Partial Fulfillment of the Requirements for the degree of

Master of Science in Aeronautics and Astronautics

School of Aeronautics & Astronautics

West Lafayette, Indiana

May 2019

THE PURDUE UNIVERSITY GRADUATE SCHOOL
STATEMENT OF COMMITTEE APPROVAL

Dr. Sally Bane, Chair

Department of Aeronautics and Astronautics

Dr. Jonathan Poggie

Department of Aeronautics and Astronautics

Dr. Sergey Macharet

Department of Aeronautics and Astronautics

Approved by:

Dr. Weinong Chen

Head of the Graduate Program

ACKNOWLEDGMENTS

I would like to take the opportunity to thank a few people who have provided me great support throughout my graduate school period at Purdue. Firstly, I would like to thank my advisor, Dr. Sally Bane, for guiding me with my research work as well as my thesis writing. Her invaluable feedback and advice helped me in getting a better understanding of both the experimental as well as the theoretical aspects of my research. Moreover, her ever-encouraging and patient nature really helped build my confidence and made the learning process very smooth and enjoyable. I would also like to express my gratitude to my other committee members, Dr. Jonathan Poggie and Dr. Sergey Macharet, for their useful suggestions towards getting better experimental results and expanding the current work.

My lab mates, Ravi, Bhavini, Prashanth, Lalit, Bang-Shuih and Nadia, have helped me a lot in so many ways. I am really grateful for everything they have done for me, from helping me with the moving and setting up of the experimental equipment to guiding me through the experiments and providing me with useful advice whenever I faced a problem. I also look up to them for their experience and helpful nature.

My family, although very far from me, have been a constant source of support and encouragement. My parents have always stressed the importance of enjoying the learning process and really understanding what I learn rather than rote learning and focusing on grades, and this held me in good stead during my time at Purdue. I will always be grateful to them for letting me explore my passions.

TABLE OF CONTENTS

LIST OF TABLES

LIST OF FIGURES

NOMENCLATURE

SDBD – Surface dielectric barrier discharge

NRP-SDBDs – nanosecond repetitively pulsed-surface dielectric barrier discharges

LAFPAs – localized arc filament plasma actuators

SWBLI – shock wave-boundary layer interactions

EHD – electrohydrodynamic

MHD – magnetohydrodynamic

MEMS – microelectromechanical systems

AC-DBD – alternating current dielectric barrier discharge

OES – optical emission spectroscopy

HV – high-voltage

ICCD – intensified charge-coupled device

PRF – pulse repetition frequency

fps – frames per second

ns – nanosecond

in. – inches

ABSTRACT

Author: Devarajan, Aarthi. MSAAE
Institution: Purdue University
Degree Received: May 2019
Title: Development of Plasma Actuators for High-Speed Flow Control Based on Nanosecond Repetitively Pulsed Dielectric Barrier Discharges
Committee Chair: Sally Bane

Over the past few decades, surface dielectric barrier discharge (SDBD) actuators have been studied extensively as aerodynamic flow control devices. There has been extensive research on producing SDBD plasmas through excitation by sinusoidal high voltage in low-speed flows, resulting in local acceleration of the flow through the electrohydrodynamic (EHD) effect. However, high-speed flow control using SDBD actuators has not been considered to the same extent. Control through thermal perturbations appears more promising than using EHD effects. SDBDs driven by nanosecond repetitively pulsed (NRP) discharges (NRP SDBDs) can produce rapid localized heating and have been used to produce better flow reattachment in high-speed flows. While surface actuators based on NRP DBDs appear promising for high-speed flow control, the physics underlying the plasma/flow coupling are not well understood and the actuators have yet to be fully characterized or optimized. In particular, methods for tailoring the plasma characteristics by varying the actuator's electrical or geometrical characteristics have not been thoroughly explored.

In the current work, NRP SDBD actuators for control of high-speed flows are developed and characterized. As discussed previously, it is believed that the mechanism for high-speed flow control by these plasmas is thermal perturbations from rapid localized heating. Therefore, the goal is to design actuators that produce well-defined filamentary discharges which provide controlled

local heating. The electrical parameters (pulse duration, PRF, and polarity) and electrode geometries are varied and the optimal configurations for producing such plasma filaments over a range of ambient pressures are identified. In particular, single and double sawtooth shaped electrodes are investigated since the enhanced electric field at the electrode tips may permit easier production of "strong" (i.e. higher temperature) filaments with well-defined spacing, even at low pressure. Time-resolved measurements of the gas temperature in the plasma will be obtained using optical emission spectroscopy (OES) to assess the thermal perturbations produced by the actuators. To the author's knowledge, these will be the first such measurements of temperature perturbations induced by NRP SDBDs. The plasma structure and temperature measurements will be correlated with schlieren visualization of the shock waves and localized flow field induced by the discharges. Finally, the optimized actuators will be integrated into a high-speed flat plate boundary layer and preliminary assessment of the effect of the plasma on the boundary layer will be conducted.

CHAPTER 1. INTRODUCTION & BACKGROUND

1.1 Motivation

The demand for air travel is fast-growing and a 2017 Press Release by the International Air Transport Association (IATA) indicated that by 2036, the number of passengers could increase almost twofold to approximately 7.8 billion [1]. According to the recent release of the special report, "Global Warming of 1.5°C" by the Intergovernmental Panel on Climate Change (IPCC), limiting global warming to 1.5°C would mean avoiding certain irreparable climatic changes. However, this would entail "rapid and far-reaching" transitions in land, energy, industry, buildings, transport and cities [2]. This would undoubtably be the case when it comes to air travel, given that the amount of fuel consumed by commercial airlines worldwide has increased by 24 billion gallons over the past 8 years [3]. Hence, improving fuel efficiency is key to alleviating the dire consequences of our current fuel consumption.

There are already certain initiatives being taken towards reducing fuel usage, emission and noise. The X-plane concepts initiated by NASA focus on innovative aircraft designs that increase lift while reducing drag and noise. Examples of these concepts include Dzyne Technologies' regional jet-sized blended wing body, which aims at making the shape of the airliner as aerodynamic as possible by creating an almost seamless line between the wing and the fuselage, and Lockheed Martin's Hybrid Wing Body, which additionally investigates the advantages of mounting the jet engines above the blended wing [4].

Apart from optimizing current airframes to improve fuel efficiency, considerable fuel reduction is being explored through alternative concepts such as electric propulsion. NASA's all-electric X-57 plane aims to "demonstrate a 500-percent increase in high-speed cruise efficiency, zero in-flight

carbon emissions, and flight that is much quieter for the community on the ground", using 14 electric motors and propellers on the final configuration [5]. Typically, supersonic commercial flights are banned due to hazards posed by the sonic boom created when the sound barrier is penetrated by the aircraft. Moreover, traveling at higher speeds adds to the fuel inefficiency. Electric propulsion could reduce the costs of cruising at high speeds, making air travel much more appealing by drastically reducing travel time. Another emerging field of research that similarly examines the use of electrical devices in conjunction with high speeds, is flow control using plasma actuators.

Plasma actuators, which are all-electric devices and do not require the use of any moving parts, are lightweight, easily reparable, and flexible [6]. By using these actuators on flaps, blades or airfoils, it is possible to either delay or induce transition of the boundary layer from laminar to turbulent. By delaying the transition from laminar to turbulent regime, skin-friction is reduced and hence drag is reduced, allowing for higher speed of flight with better fuel efficiency. By inducing turbulence, there is redistribution of momentum within the different regions of the flow and the overall energy within the boundary layer increases. This helps delay flow separation, which in turn reduces the pressure drag. With regards to high-speed flow control, it is also necessary to understand the interaction between shock waves and the boundary layer. Plasma actuators may be used to modify the high-speed boundary layer and control the shock wave structure and shock wave-boundary layer interaction (SWBLI).

A large fraction of research on plasma control of aerodynamic flows has focused on surface dielectric barrier discharge (SDBD) plasma actuators. DBD actuators lie flush with the surface and therefore do not interfere with the flow when the plasma is turned off. In addition, since DBDs are typically made up of only thin electrodes, thin layers of dielectric material and connection wires,

they are very lightweight and have no moving parts. These plasma actuators and the mechanism by which the discharges perturb the flow will be further discussed later in this chapter. In the current work, nanosecond repetitively pulsed SDBD (NRP-SDBD) actuators for control of high-speed flows are developed and characterized.

1.2 Flow control in aerodynamic applications

Flow separation and the ability to control it was the basis upon which the boundary layer theory was conceived in 1904 by Ludwig Prandtl. The presence of the boundary layer introduces several design challenges since it affects the aerodynamics and hence the performance parameters of an aircraft. Essentially, the boundary layer is a thin layer of air that flows over the wing surface. It consists of different layers of molecules, each moving with a speed faster than the layer closer to the surface. When the layers slide over each other without any exchange of molecules between contiguous layers, the boundary layer is laminar. When this stratification of the layers is disrupted by the mixing of the molecules between adjacent layers and the flow becomes random and unstable, the boundary layer is turbulent.

Boundary layer separation is a phenomenon brought about by an adverse pressure gradient, wherein a reversal of flow occurs and the wall shear stress at the point of separation goes to zero. Boundary layer separation on a wing leads to an increase in pressure/form drag and can result in stall at higher angles of attack. While separation can occur in both laminar and turbulent boundary layers, the more efficient mixing within the turbulent boundary layer increases the wall shear stress, preventing the separation which would be more likely to happen in a laminar boundary layer under similar free stream conditions. Even though the skin-friction is higher for a turbulent boundary layer, eliminating flow separation allows for a reduction in form drag and prevention of stall. Since

a turbulent boundary layer is preferred in prevention of flow separation, it is favorable to bring about an earlier transition between laminar and turbulent flow. Adding roughness to the surface is an example of "tripping" the boundary layer from the laminar to the turbulent regime. Such mechanical tripping methods are ideal for low speed flow control. However, most of the flows in aeronautical applications deal with high Reynolds (Re) numbers and hence display more turbulent attributes [7]. Since the skin-friction drag is a major contribution to the drag caused by turbulent flows, it becomes necessary to investigate ways of controlling the turbulent boundary layer as well. Hence, flow control methods are essential since they allow various types of modifications to the boundary layer.

Flow control is a field of research that has recently seen significant advances. The main goal for low-speed flow control is improving performance, especially for the start and landing phases, and this is done by controlling separation. For high-speed flow control, the main goal is to reduce drag and this is done by controlling skin friction and shock waves [8]. Mechanisms for flow control can be categorized as either passive or active. Passive control requires making geometrical alterations that are in constant operation regardless of whether these devices are required. Examples of passive control devices include vortex generators for separation control and chevrons on an exhaust nozzle for noise reduction [9]. Active control, in contrast, uses energy or momentum to modify the flow and can be activated only when flow conditions require improvement. Active control devices are preferred because they can be turned "off", unlike passive control devices which cannot be disabled and may in some cases be detrimental to the efficiency of the aircraft. For example, vortex generators would cause boundary layer transition and bring about turbulence even in cases where a laminar boundary layer is desirable for the flight conditions. One common example of an active control method is 'Oscillatory blowing and suction'. In this approach, fluid is extracted from the

boundary layer using suction before it separates upstream, while blowing is used to increase the momentum of the boundary layer by inserting fluid into it. This blowing and suction flow control process is an oscillatory one and one way of achieving it is using a synthetic jet [10]. Studies by Yousefi et al. [11] have found that perpendicular suction at the leading edge and tangential blowing at the trailing edge are the best locations for suction and blowing jet slots. DBD plasma actuators can also be used to increase the momentum within the boundary layer. Figure 1.1 illustrates the mechanism through which synthetic jets and DBD plasma actuators achieve a highly energized boundary layer [12]. As can be seen from Figure 1.1, the synthetic jet actuator increases the momentum in the direction normal to the surface whereas the DBD plasma actuator increases the momentum tangential to the surface.

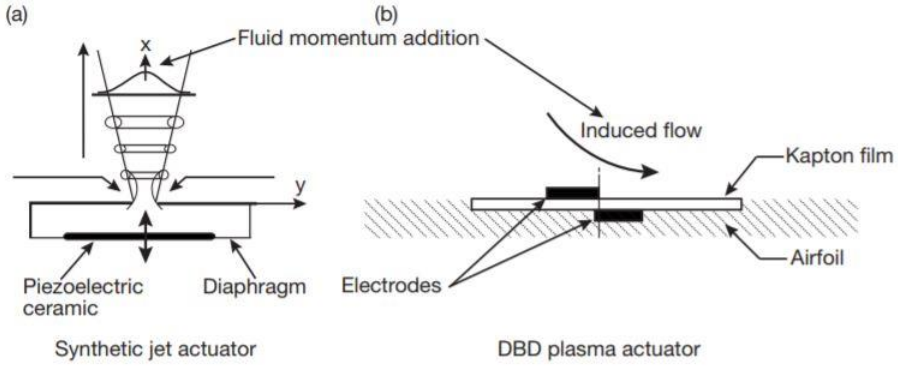

Figure 1.1: Schematic of (a) a synthetic jet actuator [13] and (b) a plasma actuator [14], including the direction of the net fluid momentum addition [12].

These approaches, while proven to have significant flow control authority in low-speed and low-Reynolds number flows, have not been as successfully applied for high-speed and high Reynolds number flows. The amplitude, bandwidth and phasing attributes of these actuators do not appear to demonstrate the same efficiency in controlling high-speed flows [15]. Momentum and instability frequencies increase as the Reynolds number of the flow increases. To effectively control the flow,

actuators must be able to produce flow excitation with much higher amplitudes and frequencies, which are conflicting requirements [16]. Hence, most active flow control methods become inapplicable to high-speed flows. However, recent studies have shown that there are a few exceptions. Steady micro-jets, localized arc filament plasma actuators (LAFPAs), and pulse detonation actuators are some of the few active flow control devices that have been investigated at supersonic speeds [12]. For example, LAFPAs, a class of plasma actuators, have been used to produce perturbations at high amplitudes and high forcing frequencies up to 100 kHz, while operating at a low plasma power [17].

When considering high-speed flows, it is necessary to investigate the shock wave-boundary layer interactions (SWBLI) [18] which are ubiquitous in both internal and external flow problems in high-speed flight. One example where SWBLI are critical to performance are supersonic mixed-compression inlets. The flow separation that occurs due to these interactions causes a reduction in the effective area of the inlet [19]. This amounts to a decrease in the mass flow that goes to the engine and reducing efficiency of the system. The flow separation also causes unsteadiness and significant pressure load fluctuations which can result in damage to parts of the engine. Therefore, it is important to consider the impact of shock waves in flow control of supersonic flows. One method that has been used to prevent separation in supersonic inlets is boundary layer bleed, where low momentum fluid within the boundary layer is removed. However, this method is not very efficient in terms of improving overall engine performance as the "bleeding" process requires additional energy and reduced mass flow, whereas the bleed and dumping systems add to the weight and drag of the inlet [20].

1.3 Plasma Flow Control

1.3.1 Plasma Control Mechanisms

Plasma flow control is governed by three main mechanisms – electrohydrodynamic (EHD) forces, magnetohydrodynamic (MHD) forces, and thermal heating. The EHD and MHD forcing mechanisms work by momentum transfer through collisions from charged species that are accelerated by Coulomb and Lorentz forces. By flow entrainment, these forces increase the momentum in the boundary layer. EHD forces require high levels of ion density to influence the flow and only have a significant effect on the boundary layer at flow velocities of 30-100 ms^{-1} [21]. Also, flow control using MHD forces require high flow conductivities and hence very low-pressure environments [22]. The acceleration produced by the EHD effect does not add enough momentum to the boundary layer at flow velocities above 30 ms^{-1}. Control of high-speed flows using electric and magnetic fields would require huge power inputs because only a small part of the power input, usually below 1%, goes to the direct momentum transfer between the charged and neutral species [23]. Even with the resulting low ionization fraction allowing for interaction between the electrons and ions and the electromagnetic fields, the momentum transfer would not be great enough to effect change on high-speed flows that have much greater momentum and energy [24].

Control using localized thermal perturbations appears more promising for high-speed flows. Flow perturbations caused by localized heating can be grouped into three types – compression waves, stochastic perturbations (small-scale), and coherent structures (large-scale). Recent studies on plasma-induced compression waves have shown that generation of these waves would require a large fraction of the plasma discharge energy to be converted to heat within a short time frame, producing an increase of the gas temperature close to 200 K [25]. The rapid localized heating caused by constricted/filamentary plasma discharges leads to an abrupt jump in pressure close to

the filaments, producing strong compression waves. These waves can produce vortices that enhance mixing and redistribution of momentum within the boundary layer. Thus, these rapidly heated near-surface regions essentially behave in a similar way to geometrical alterations such as tabs and cutouts [26]. "Thermally-based" flow control through localized energy deposition seems to be a more robust approach for high-speed flows, however, the working principles of the mechanism require more in-depth understanding [27].

1.3.2 Arc Filament Plasma Actuators

Active control can also be categorized according to the mechanism used to control the flow [28]. The first category involves injection of momentum to energize low momentum, near-surface flow or production of body force using additional flow structures. In the second category, perturbations are introduced that are within the range of frequencies and modes of the known flow instabilities, thereby exciting them. The second category is preferred for high-speed and high-Reynolds number flow control due to the great energy input demands. Actuators for high-speed flow control should be able to make full use of the formation of streamwise vortices and manipulate the naturally-occurring instabilities in the flow. Providing high amplitude and bandwidth forcing, without protruding into and interfering with the flow, would also be an ideal characteristic of high-speed plasma actuators [22].

Such characteristics have been achieved with arc filaments actuators. In these actuators, a high voltage is applied across a gap between two electrodes to produce a plasma arc [29]. A conductive channel is created by an electron avalanche and the ionization rate is increased by the thermionic effect [30, 31]. LAFPAs, a type of arc filament actuator, have been studied extensively in applications involving supersonic flow, such as starting issues in supersonic inlets and

enhancement of mixing in supersonic combustors. LAFPAs have benefits such as ease of control and allowing phase-control and excitation or dampening of different azimuthal modes. These actuators were originally developed by researchers at The Ohio State University to enhance mixing and mitigate noise for high-speed flow control [32]. The actuators influence the flow by amplifying the natural instabilities within the flow. These actuators produce constricted, or filamentary plasma discharges, which produce the required strong localized heating and pressure perturbations [33], in contrast to glow discharge plasma.

Leonov et al. investigated the use of an array of quasi-DC filamentary discharges in controlling the performance of a supersonic diffuser and improving the efficiency of supersonic combustors and found that the plasma produced significant modifications to the topology of the flow [34, 35]. Oblique shock/boundary layer interaction has also been studied using DC arc discharges by Bianchi et al. [36]. As shown in Figure 1.2, an array of three electrode pairs was placed 10mm upstream of a compression ramp with a 23.5° wedge angle. The array was placed at the point where the oblique shock wave originated. It was observed that the turbulent structures in the separated flow after the shock wave could be modified, even with the low energy of 100 mJ per pulse applied to the three actuators. The conclusions reached were important in understanding a potential approach for controlling supersonic flow, while minimizing the energy cost. Similarly, Wang et al. [37] studied the effect of arc discharge plasmas on the oblique shock wave produced by a wedge in supersonic flow and found that the thermal effect dominant and a thermal chocking model could be used to rationalize the upstream shift, angle decrease and weakened intensity of the shock. Sun and co-workers studied surface quasi-DC arc discharges with millisecond and microsecond actuation in quiescent air and supersonic flow [38]. They discovered that the thermal mechanism was the main mechanism controlling the boundary layer separation by impinging shocks. They

also used similar discharges in studying detached shocks for a blunt body [39] and a supersonic airfoil [40] and found that arc plasma actuation could be used to manipulate the stand-off distance and strengths of the shocks. These studies are promising because they demonstrate that plasma discharges, when restricted to a specific location with respect to the shock wave, can provide control authority in supersonic flows with modest energy input. While these studies use quasi-DC plasmas, in recent years interest has increased in using ultra-short (nanosecond duration) pulsed plasmas produced at high repetition rates, as discussed in the next section.

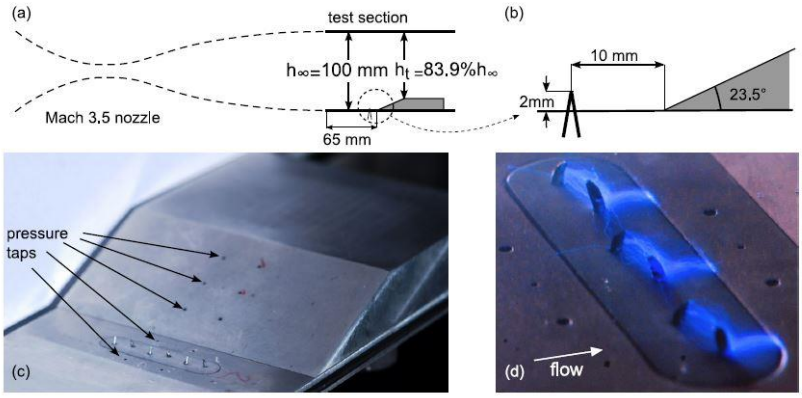

Figure 1.2: Schematics of the wind tunnel setup - (a) nozzle and test section, (b) streamwise electrodes arrangement, (c) measurement locations, (d) discharges at Mach 3.3 [36].

1.3.3 Nanosecond Repetitively Pulsed Dielectric Barrier Discharges

There has been extensive research on producing SDBD plasmas through excitation by sinusoidal high voltage in low-speed flows, resulting in local acceleration of the flow through the EHD effect. The AC-driven discharge formation produces an ionic wind, which induces flow reattachment by adding momentum to the boundary layer. High-speed flow control using SDBD actuators has not been explored to the same extent as low-speed flow control. SDBD plasmas produced by AC

voltage waveforms are typically near room temperature. NRP-SDBD actuators can produce rapid localized heating and have been used to produce better flow reattachment in high-speed flows with Mach numbers up to 0.85 [41]. Since plasma-based actuators have shown significant promise in comparison to other flow control methods such as mechanical devices, wall synthetic jets, or MEMS [42], it is important to understand how to bridge the gaps in knowledge regarding adapting SDBD plasma actuators to high-speed flow control. Using short pulses to drive the DBD pulses, as with NRP-DBD actuators, can address some of the limitations of traditional AC-DBD actuators for high-speed flow control [16], and previous studies have shown that such actuators can be efficient in controlling high-Reynolds number turbulent shear layers [25]. NRP discharges are driven using a series of pulses that are characterized by their peak voltage, pulse duration and pulse repetition frequency. Unlike the homogenous and uniform plasma discharges typically formed in DBDs driven by an AC power source, NRP-DBD discharges tend to be more filamentary and thus may produce the same control mechanisms as LAFPAs [40]. Flow control by thermal perturbations occurs due to the filamentary nature of these NRP discharges.

In recent studies by Nishihara et al. [43, 44], plasmas generated by NRP SDBDs were used to modify shock wave structure and shock wave-boundary layer interaction (SWBLI) in supersonic flows. In the first study, an NRP-SDBD actuator mounted on the surface of a cylinder in Mach 5 flow was used to control the stand-off distance of the bow shock [43]. In a later study, they investigated the control of shock wave/boundary layer interaction on 12° and 22° wedges in Mach 2.2 flow [44]. Perturbations of the incident and reflected shock were observed due to the compression waves produced by the plasma interacting with the separated flow. Also, the plasma was found to excite low-frequency oscillations in the separation bubble. Recently, Kinefuchi et al. [45] used three different NRP-SDBD electrode configurations to study the effect on an

impinging shock on a lower wall boundary layer. In one particular configuration, favorable downstream motion of the reflected shock and suppression of SWBLI was observed, and the authors postulated that the effect was due to vorticity generation near the surface by the plasma instead of direct gas heating. While surface actuators based on NRP-DBDs appear promising for high-speed flow control, the physics underlying the plasma/flow coupling are not well understood and the actuators have yet to be fully characterized or optimized. In particular, methods for tailoring the plasma characteristics by varying the actuator's electrical or geometrical characteristics have not been thoroughly explored.

A limited number of prior studies have investigated the effect of electrical and geometrical parameters on SDBDs driven by nanosecond-scale pulses. Electrical parameters that have been investigated include applied voltage amplitude and polarity, pulse duration, and energy deposited in the gas. The effect of applied voltage has been investigated in some studies. Yang et al. [46] studied the effect of pulse peak voltage on the intensity and spatial distribution of emission by the nitrogen second positive system. They found that as the peak voltage increases, both the light emission intensity of $N_2(C^3\Pi_u \rightarrow B^3\Pi_g)$ and the plasma area on the surface of the dielectric plate increases in the horizontal direction. Opaits et al. [47] experimented with different voltage waveforms and found that the new voltage profile which consists of nanosecond pulses superimposed on a high-voltage low frequency sinusoidal bias voltage leads to higher actuator performance. The effect of pulse polarity was investigated in two studies. Gibalov et al. [48] found that when the cathode is encapsulated in the dielectric material, there is a greater tendency for filamentation to occur than when the anode is encapsulated. Starikovskii et al. [49] also noted that the discharge propagation velocity is lower when the anode is covered by the dielectric. In prior work in our lab, Newnam [50] investigated the effect varying the pulse duration had on the plasma

formation in a traditional SDBD configuration. For a fixed applied voltage and PRF, as the pulse duration was increased, the plasma transitioned from a quasi-homogenous, diffuse plasma to a more filamentary plasma. Newnam thus concluded that pulse duration was an additional parameter that could be varied to produce the desired plasma characteristics. Wang and Roy postulated that the energy deposited by the discharge is the most important parameter for assessing effectiveness of the actuator [51]. Their experimental measurements showed that the mean temperature values can reach 400 K for 50 ns pulse durations and that such fast heating of the gas layer leads to periodic flow disturbances that can be used to control boundary layer separation.

In addition to the electrical parameters, the electrode geometry and material and ambient conditions will also influence the plasma characteristics. For example, SDBDs driven by NRP discharges in a three-electrode configuration, called sliding discharges, have been shown to produce higher flow velocities and body force than traditional two-electrode DBD actuators [52]. Yang et al. [45] studied production of diffuse plasma using nanosecond-pulsed DBDs with a needle array-plate electrode configuration, where the number of needles, angle of the needles to the horizontal and the electrode distance were varied to assess the effect on the plasma. Regarding the effect of ambient conditions, Starikovskii et al. [48] found that the plasma becomes more uniform and homogenous as the pressure decreases. They also found that as pressure increases, the electric field between the electrodes is reduced and thus the filamentation is likely to become less defined and more diffuse. Overall, investigations on the effect of electrode geometry and ambient conditions on NRP-driven SDBDs have thus far been very limited.

1.3.4 Temperature measurements of SDBD plasma discharges

As stated previously, recent work postulates that rapid heating by the plasma may provide a mechanism for flow control at high speeds and Reynolds numbers. However, measurements of the thermal characteristics of SDBD plasma discharges have been somewhat limited. There have been a small number of studies on the temperature rise produced by AC-DBD plasmas. Infrared thermography was used by Tirumala et al. [53] to study the temperature distribution on the surface of a DBD actuator, while varying geometrical and electrical parameters. A hypothesis regarding the relationship between the dielectric surface and the gas temperatures was proposed. Infra-red thermal imaging was also used by Joussot et al. [54] to study the dielectric surface temperature on a continuously operating DBD actuator, in both quiescent and an external flow. In quiescent flow, there was a rapid and significant increase of 50°C in the dielectric temperature at the point when the discharge was ignited. However, when an external flow was introduced, there was a decrease in the dielectric temperature due to heat dissipation. Cold wire anemometry (CWA) was used by Jukes et al. [55, 56] to measure the temperature of the induced flow by an AC-DBD actuator. A very small temperature increase of 2°C was registered in the flow, indicating the non-thermal characteristic of an AC-DBD. Optical emission spectroscopy (OES) was used by Dong et al. [57] and Stanfield et al. [58] to measure the plasma rotational and vibrational temperatures above the grounded electrode. Dong and co-workers [56] measured a moderate rise in the rotational temperature that increased with the frequency of the driving AC high voltage (380 K and 420 K for 1 and 2 kHz, respectively). They also measured a significantly higher vibrational temperature (3000 K) that did not depend on the frequency. Stanfield et al. [57] measured rotational and vibrational temperatures and found that both the temperatures increased with increasing voltage, with maximum values of 390 K and 3250 K, respectively. For NRP-DBD plasmas, most studies have considered schlieren imaging as a thermal characterization technique but explicit temperature

measurements cannot be derived [59]. For example, in a study by Correale et al. [60], schlieren visualization showed a strong region of hot gas that persisted after the departure of the plasma-induced shock wave, as shown in Figure 1.3.

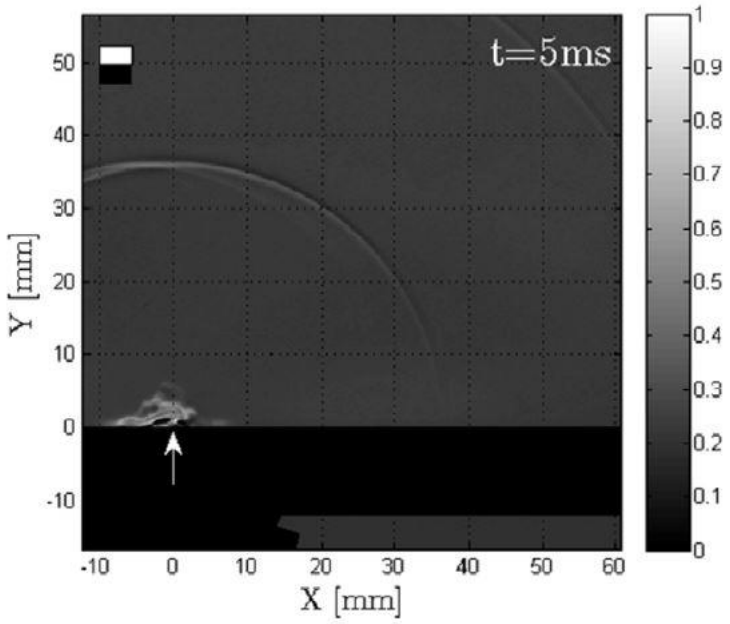

Figure 1.3: Schlieren imaging of NRP-DBD actuation – 50 pulses at 10kHz. Much after the last compression wave is generated, there is still a region of hot gas shown [60].

The only quantitative measurements of NRP-DBD plasma temperature were obtained by Starikovskii et al. [61] and Takashima et al. [62] using OES. Starikovskii et al. [61] measured the temperature rise from a single pulse (PRF of 1 kHz), 25 ns in duration with 14 kV peak voltage, to be 40 K (increase from 290 K to 330 K during the discharge). Takashima et al. [62] used a floating tip electrode to promote filamentary breakdown to a rectangular grounded electrode. They measured the temperature of a single discharge within a 50-pulse burst PRF of 10 kHz and pulse duration of 50 – 100 ns and found that rotational temperature ranged approximately 380 K (1st pulse) to 450 K (50th pulse). There is a general lack of data on the temperature profile of NRP-

DBDs and this information is especially essential in order to be able to draw conclusions on the thermal effect of these discharges on high-speed flow.

In the current work, NRP SDBD actuators for control of high-speed flows are developed and characterized. As discussed previously, it is believed that the mechanism for high-speed flow control by these plasmas is thermal perturbations from rapid localized heating. Therefore, the goal is to design actuators that produce well-defined filamentary discharges which provide controlled local heating. The electrical parameters (pulse duration, PRF, and polarity) and electrode geometries are varied and the optimal configurations for producing such plasma filaments over a range of ambient pressures are identified. In particular, single and double sawtooth shaped electrodes are investigated since the enhanced electric field at the electrode tips may permit easier production of "strong" (i.e. higher temperature) filaments with well-defined spacing, even at low pressure. Time-resolved measurements of the gas temperature in the plasma will be obtained using OES to assess the thermal perturbations produced by the actuators. There is a need to understand if the strength of the filaments is linked to their brightness or intensity and in turn, if there is a correlation between the intensity and the temperature of these discharges. The effect of varying the plasma electrical parameters on the temperature profile of the filamentary discharges is also investigated using OES. The localized flow field induced by the discharges on quiescent air and the effect of the discharges on the shock waves generated in supersonic flow are studied using schlieren visualization.

CHAPTER 2. EXPERIMENTAL METHODS

2.1 Plasma Generation

The SDBD plasma actuator has a typical asymmetric electrode geometry like that shown in Figure 2.1 and the plasma is excited by nanosecond, high-voltage (HV) pulses. Copper foil of thickness 0.0035 in. and width 0.5 in. is used for the electrodes and 0.0025 in. thick Kapton tape is used as the barrier layer between the electrodes. For the first few electrode geometries, two layers of the dielectric tape are used. In the cases where arcing of the plasma filaments was often observed, e.g. the single and double saw tooth electrodes with no gap between the electrodes, three layers of tape are used. For benchtop tests and plasma visualization, the actuator is mounted onto a flat 0.25 in. acrylic plate.

Several different DBD actuator configurations are considered in this work. The most common SDBD electrode configuration, which was investigated previously by Newnam [50], uses two parallel strips of the copper tape mounted flush with one another, with one strip buried under dielectric tape and the other exposed, as shown in Figure 2.1. In the current work, saw tooth electrodes are explored to promote plasma filamentation and to control the number of plasma filaments. Configurations with a single saw tooth and double saw tooth are investigated, and effects of removing the dielectric barrier and including an interelectrode gap are explored. Effect of ambient pressure variation is also investigated, whereby the actuator is placed within a pressure vessel as shown in Figure 2.2. Details on the various electrode configurations and optimization of the actuator design are given in the next chapter.

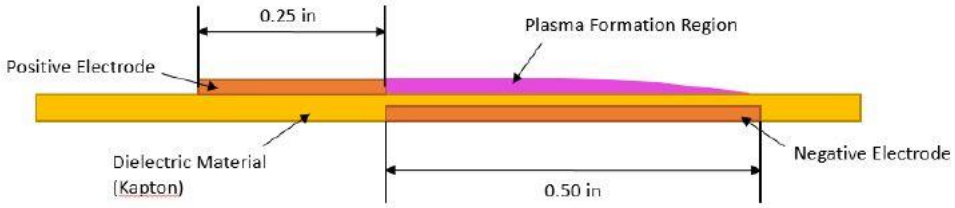

Figure 2.1: Schematic of a typical surface DBD actuator.

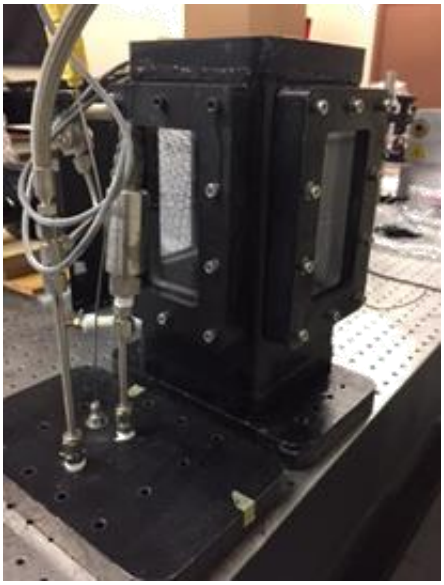

Figure 2.2: Pressure vessel used to conduct experiments with ambient pressure variation.

A custom high-voltage pulser (Eagle Harbor Technologies NSP-300) is used to generate the nanosecond duration pulses driving the plasma formation. The pulser allows pulse parameters to be controlled individually – the applied voltage can be set up to a maximum of 20 kV, pulse duration can be set within the range of 20-110 ns, and pulse repetition frequency can be set up to 100 kHz in the continuous mode and 400 kHz in the burst mode. While a typical surface DBD actuator operates with one active and one grounded electrode, the actuator in this case has the

electrodes at equal positive and negative potentials since the pulser has a floating ground. The plasma is visualized using an ICCD camera (Princeton Instruments PI-MAX 4).

2.2 Plasma Visualization and Temperature Measurement

Temperature measurements are critical to better understand the thermal perturbations induced by NRP SDBDs. Optical emission spectroscopy (OES) will be used to measure the temperature of the plasma filaments produced by the NRP DBD actuator. A schematic of the experimental setup for the OES measurements is shown in Figure 2.3. The plasma discharge is generated between the two electrodes of the actuator. The emission from one plasma filament is collimated and focused onto the entrance slit of a Princeton Instruments 2500i spectrometer using two off-axis parabolic (OAP) mirrors of 2 in. reflected focal length. The light enters the spectrometer and passes through a grating, which separates it into the different spectral wavelengths. An ICCD camera is directly connected to the spectrometer and serves as the detector to measure the intensity of the specific wavelengths of light. Precise alignment of the optical system is critical to maximize the light intensity ultimately reaching the ICCD camera. The peak signals of the spectral lines are collected by the camera and processed to generate a spectrum of light intensity peaks against the wavelengths. The measured spectrum is then fitted against a predicted numerical model in Specair24 software to obtain the rotational and vibrational temperatures of the plasma.

First, a mercury lamp is used to obtain a predefined calibration of the system to account for instrument broadening of the spectra. Next, light from a green LED is collimated and focused onto the spectrometer slit for characterizing the system and to find the most suitable parameters or settings to obtaining data for the plasma discharges. The dispersed LED signal is focused onto the slit, which can be adjusted to control the spatial resolution of the probe volume. The spectrometer

slit distance is set to 20 μm. The signal throughput is maximized by adjusting the height of the spectrometer relative to the camera and the distance between the spectrometer and the camera lens. The LED source is then replaced by a pin-to-pin electrode configuration to collect data for a single filamentary discharge. The spectra obtained at different wavelengths is used to understand the best parameters to be used for capturing a strong signal from plasma discharges. Finally, the double saw tooth DBD electrode configuration is placed at the location of the pin-to-pin electrode configuration, such that the point where a plasma filament is formed at one of the teeth coincides with the point where the spark was formed on the pin-to-pin configuration.

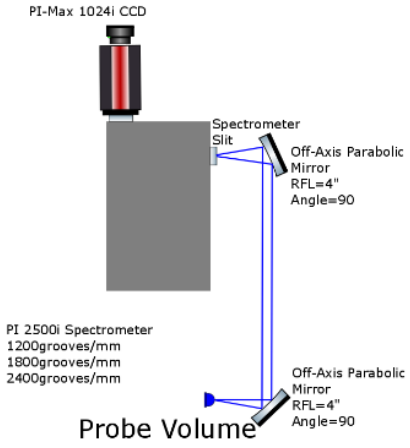

Figure 2.3: Schematic of the OES experimental setup for temperature measurements.

Voltage and current measurements are taken, using two high voltage probes and a high bandwidth current transformer, on the Agilent Technologies Infinium DSO9104A oscilloscope. These measurements are useful in the calculation of the pulse energy, which is a critical parameter required to quantify the efficiency of the plasma actuator. An example of a trace for a single pulse of pulse duration 50 ns and PRF 25 kHz is shown in Figure 2.4, where the approximate peak pulse voltage and current are 7.6 kV and 33 A, respectively.

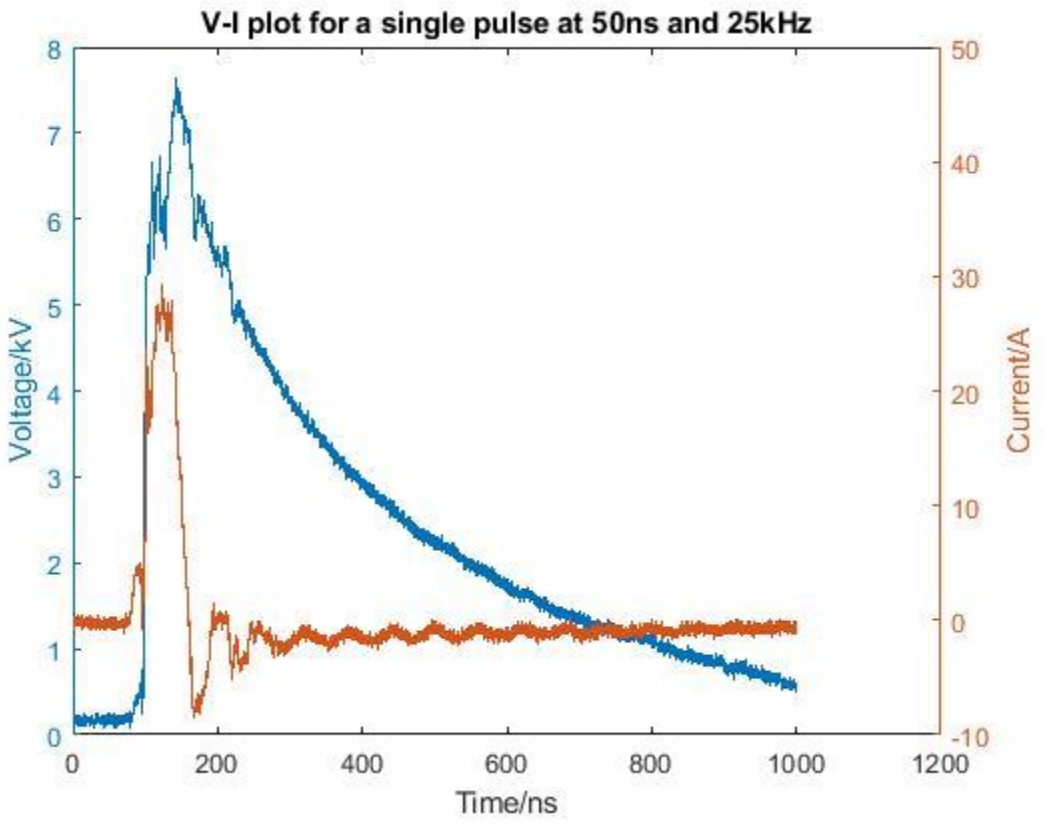

Figure 2.4: An example of a V-I plot for a single pulse with a pulse duration of 50 ns and a PRF of 25 kHz.

2.3 Schlieren Imaging of Induced Flow

The shock wave and subsequent flow produced by the ns-DBD is visualized using a high-speed schlieren system. A schematic of the modified Z-type schlieren system used is shown in Figure 2.5. A 150 W xenon arc lamp (Newport 66907), 60 mm aspheric condenser lens and pinhole are used to create an approximate point light source. Collimation and convergence of the light beam onto a knife edge is accomplished using two 6 in. diameter concave mirrors with a focal length of 120 in. To reduce light spillage, the angle of the ray cone emitted from the light source is controlled using an intermediate lens before the collimating mirror. The schlieren images are recorded using a Photron FASTCAM SA-Z camera at a frame rate of 20,000 fps with a 1024 x 1024 pixel resolution.

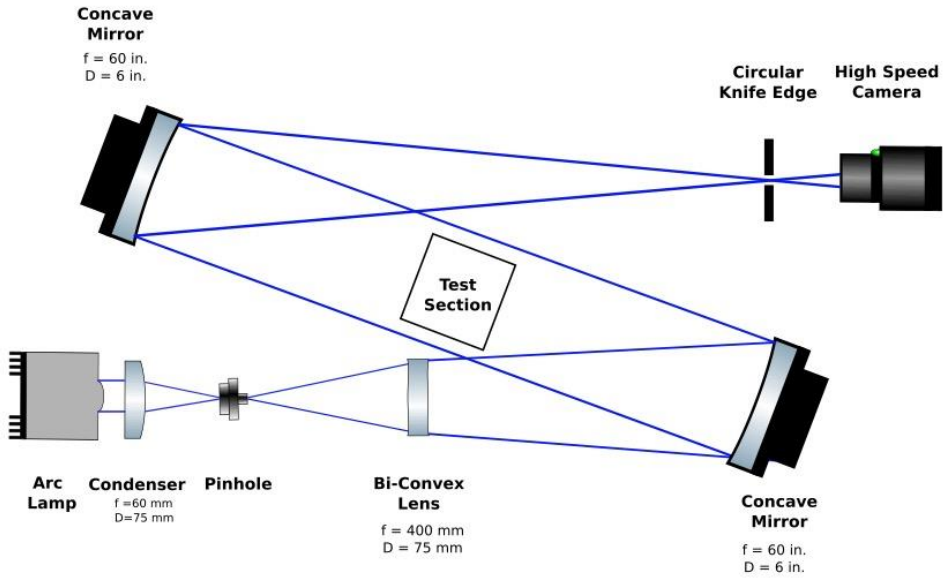

Figure 2.5: Schematic of the schlieren system used to visualize the shock waves and flow induced by the ns-DBD plasma.

2.4 Supersonic Wind Tunnel Experiment

To study the ns-DBD plasma in a high-speed flow, experiments are performed in the blowdown supersonic wind tunnel at Purdue University's Aerospace Sciences Laboratory shown in Figure 2.6. The tunnel has four different nozzles for operation at Mach numbers of 0.6, 2.0, 2.5, and 3.6 with a run time of 30 seconds. The test section is 1.75 in. by 2.25 in. and has a 3 in. diameter window for schlieren visualization. The supersonic wind tunnel also has a basic schlieren system for visualizing the flow in the 3 in. field of view of the side wall window. The Mach 2.0 nozzle is used to run the supersonic flow tests. To investigate the effect of the plasma on a shock wave, the actuator is mounted onto a ramp model, where the ramp can be shifted to various positions with respect to the plasma location. Also, the ramp can be removed to study the plasma effect on an undisturbed boundary layer. The current version of the ramp model is shown in Figure 2.7.

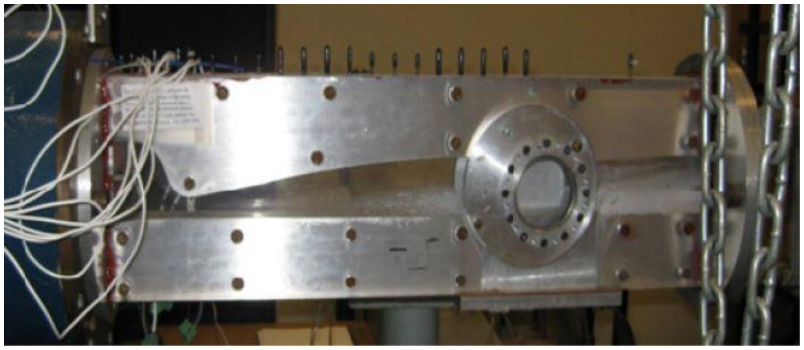

Figure 2.6: Mach 2.5 nozzle and test section of the blowdown supersonic wind tunnel at Purdue University's Aerospace Sciences Laboratory.

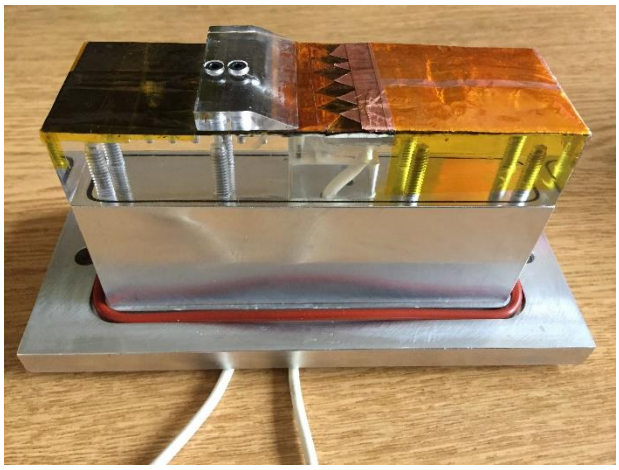

Figure 2.7: Ramp model used for tunnel testing, with DBD actuator mounted on the surface.

CHAPTER 3. RESULTS AND DISCUSSION

Experiments were conducted to characterize the nanosecond repetitively-pulsed dielectric barrier discharge (NRP-DBD) formed in both ambient conditions and high-speed flow. Characterization of the plasma discharge involved studying the structure of the filaments formed as well as taking temperature measurements of the discharge. Initial table-top experiments in ambient conditions were conducted for this purpose. For the preliminary tests conducted to determine the optimized electrode configuration, these pulse parameters were investigated – pulse durations in the range of 35-110 ns and pulse repetition frequencies (PRFs) in the range of 200-300 Hz for geometries without the use of a dielectric barrier and 25-80 kHz for geometries with a dielectric barrier. The effect of ambient pressure variation on the plasma was also studied for the different electrode configurations. The pressures studied ranged from 2.7 psi to 3 atm.

Upon identifying the optimized electrode configuration for the NRP-DBD actuator, characterization of the plasma formed involved studying the effect of the discharge on quiescent air using schlieren visualization. Furthermore, temperature measurements of the discharge were taken using optical emission spectroscopy (OES) to gain a better understanding of the thermal mechanism behind flow control using NRP-DBD actuators. The optimized electrode configuration was also placed in a supersonic tunnel to study the effect of high-speed flow on the structure of the filaments formed.

3.1 Electrode Optimization

In a study done by Cui et al. [63] on the configurations of NRP-DBD actuators, they compared a comb-shaped DBD actuator with the straight asymmetrical one and found that a more distinct shock wave was formed in the case of the former actuator. They concluded that layout of the

actuator plays a critical role in determining the electric potential between the exposed and buried electrodes and hence, the formation of shock waves. Since the forcing mechanisms are fundamentally different for AC-DBD and NRP-DBD actuators, the layout of the NRP-DBD actuators need not necessarily be the same as that of the conventional layout used in AC-DBD actuators. Therefore, it is important to gain an understanding of how actuator configurations can affect the plasma discharge formed in NRP-DBD actuators. Thomas et al. [64] studied the effect of electrode geometry as a part of an investigation to find the optimized AC-DBD plasma actuator for active flow control. They compared the use of a serrated electrode with the conventional flat one and found that there was a significant increase in the body force with plasma generated using the serrated electrode. This is shown in Figure 3.1, where the actuator with the serrated electrode generated a higher thrust value than the actuator with the straight electrode, at any given applied voltage. Hence a similar electrode geometry to the serrated one, where sharp points can induce localized plasma discharges, can be investigated for NRP-DBD actuators to understand if there would be a similar improvement in the forcing mechanism unique to that of these discharges, i.e. thermal perturbations.

As discussed previously, the mechanism for flow control using NRP discharges is believed to be rapid localized heating by the plasma. To maximize this effect, it is desirable that the plasma be produced in a filamentary regime where the temperature increase will be significantly higher than with a diffuse, "glow"-like discharge. Therefore, the objective in the current work is to design electrode configurations that produce highly filamentary discharges at both atmospheric pressure and at lower pressures typical of many supersonic aerodynamic applications. We propose using single and double sawtooth shaped electrodes to promote filamentation by enhancing the electric field and to control the number and spacing of the plasma filaments. We also consider the effect

of a gap between the electrodes and the effect of a dielectric barrier separating the electrodes on the plasma produced. In addition, the electrical parameters driving the discharge are varied, specifically the pulse duration, PRF and polarity. Finally, the effect of reducing the ambient pressure on the plasma structure is also investigated.

Schematics of the six different electrode configurations explored in this work are shown in Figure 3.2. Two electrode shapes are considered: single sawtooth with rectangular electrode and double sawtooth. These electrode shapes were tested using a dielectric barrier with 1) no gap between the electrodes and 2) with a 0.25 inch gap. In addition, both electrode shapes were tested without the dielectric barrier with and without the gap between the electrodes. These configurations are labeled (1) – (6) in Figure 6. In the current experiments, the peak pulse voltage is kept constant at 400 V for all tests, while the pulse duration and PRF are varied. A burst of 200 pulses at the desired pulse repetition rate are sent to the actuator and one trigger pulse is sent to the camera.

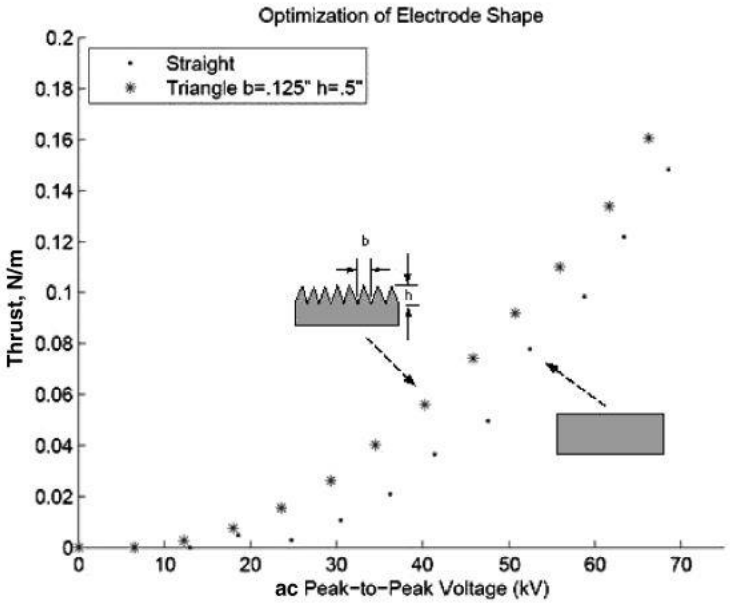

Figure 3.1: Thrust per unit span for straight and serrated electrodes in an AC-DBD actuator [64].

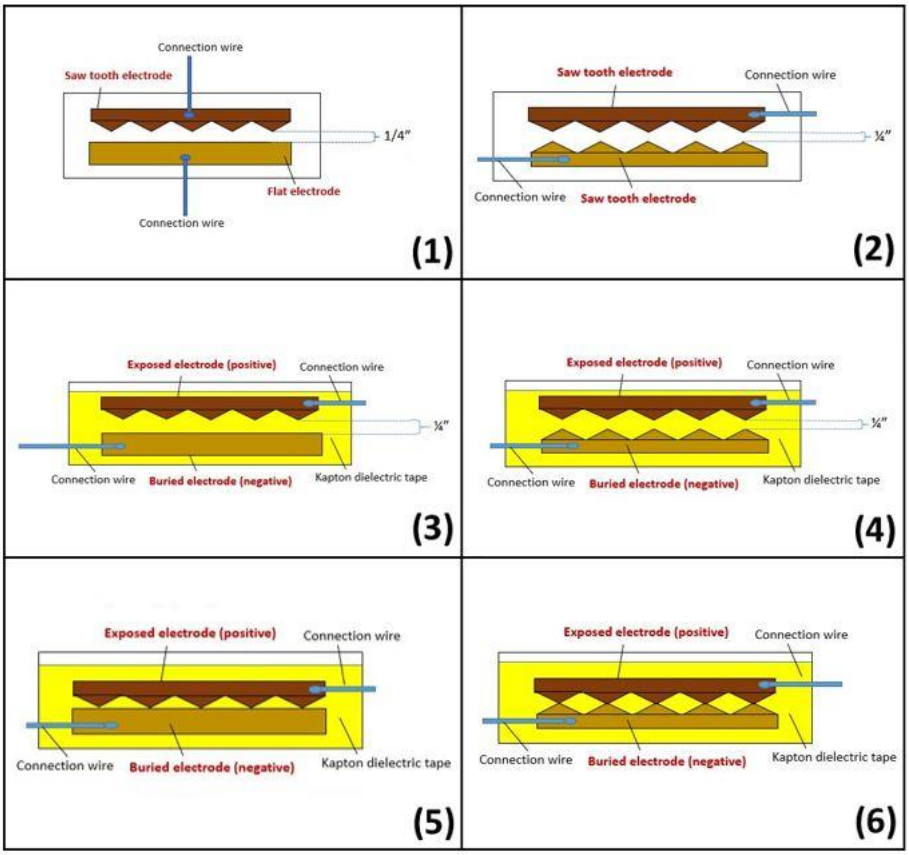

Figure 3.2: Schematics of the six electrode configurations considered in this work.

3.1.1 Electrode Geometry and Pulse Parameters

Configurations 1 and 2

In configurations 1 and 2, there is a 0.25 inch gap between the single (1) and double (2) sawtooth electrodes and no dielectric barrier. For the configurations without a dielectric barrier, the PRF had to be kept to a few hundred Hz to prevent significant arcing. For the single sawtooth configuration (1), faint uniform plasma filaments were observed at low pulse duration (30 ns) and a PRF of 250 Hz, but arcing occurred at one electrode tooth for higher pulse durations and frequencies. Arcing began for a pulse duration of 35 ns, as shown in Figure 3.3, and continued for higher values. For the double sawtooth electrodes as in configuration (2), faint uniform plasma

filaments are formed between each sawtooth pair, as shown in Figure 3.4. As pulse duration increased, the filaments became slightly brighter and eventually arcing was observed on one tooth pair. For each pulse duration, varying the frequency had little noticeable effect on the plasma filaments. The images in Figures 3.3 and 3.4 were captured using the Photron FASTCAM SA-Z camera at a frame of 250 fps and 500 fps respectively, with a frame exposure time of 1/1000 s. However, the filaments formed were faint and the images had to be processed to view the filaments. Hence, the ICCD camera (Princeton Instruments PI-MAX 4) was used to capture more intensified images of the filaments. The images in Figure 3.5 were captured with the gain set to 1, gate delay set to 250 ns and gate width set to 1 ms.

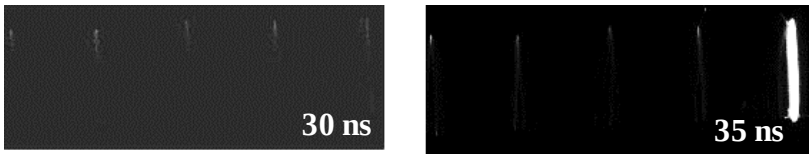

Figure 3.3: High-speed camera images of uniform faint plasma filaments formed in electrode configuration (1) at PRF of 250 Hz and varying pulse durations.

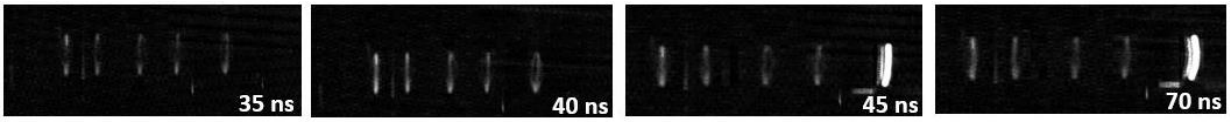

Figure 3.4: High-speed camera images of uniform plasma filaments formed in electrode configuration (2) at PRF of 250 Hz and varying pulse durations.

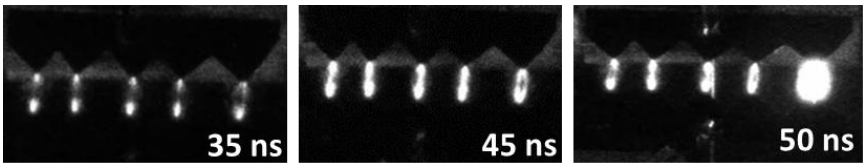

Figure 3.5: ICCD images of uniform plasma filaments formed in electrode configuration (2) at PRF of 250 Hz and varying pulse durations.

Configurations 3 and 4 – Effect of dielectric barrier

In configurations 3 and 4, there is a 0.25 inch gap between the electrodes and one electrode is encapsulated in a dielectric barrier. For both the single and double sawtooth configurations, filaments are formed at each tooth as in configuration 2 with no dielectric barrier. However, with the barrier present, the filaments are more well-defined, often with multiple branches, as shown in Figures 3.7 to 3.9, and can extend past the tip of the teeth on the negative electrode. In the study mentioned at the beginning, which compared the typical flat electrode actuator geometry with a comb-shaped geometry, a similar plasma formation was observed as shown in Figure 3.6. The comb-shaped electrode is made up of 13 wires of 0.7 mm diameter and there is a gap of 4 mm between the flat and comb-shaped electrodes. The plasma filaments formed in the case of the comb-shaped layout tend to spread and look more branched outwards compared to the straight filaments formed on the flat electrode layout. The wire tips on the comb-shaped electrode and the saw tooth tips on the saw tooth electrode would have a higher potential and the filaments would be expected to extend out only from those tips. The same level of branching is not observed in configurations 1 and 2, hence the spreading out of the charges by the introduction of the dielectric barrier may be the reason for the more defined branching in configurations 3 and 4.

In the single electrode configuration, the number of filaments and their emission intensity depended strongly on the pulse parameters, both increasing with increasing pulse duration and PRF, as seen in Figure 3.7. In the double sawtooth case, however, the effect of pulse parameters on the plasma was less apparent as shown in Figure 3.8. The images in Figure 3.7 were captured using the Photron FASTCAM SA-Z camera at a frame of 25000 fps for the 25 kHz tests and 50400 fps for the 50 kHz and 80 kHz tests. The frame exposure time was set to 1/26047 s for the 25 kHz tests and 1/54842 s for the 50 kHz and 80 kHz tests. The images in Figure 3.8 were captured using

the SA-Z camera at a frame rate of 50400 fps and a frame exposure time of 1/54842 s. These images in Figure 3.9 were captured using the ICCD camera, where a gain of 50 is used. The gate delay and gate width on the ICCD camera are set to 250 ns and 1 ms, respectively.

Figure 3.6: Plasma formation on conventional DBD actuator layout (left) and on comb-shaped DBD actuator layout (right) at a repetition frequency of 100 Hz [63].

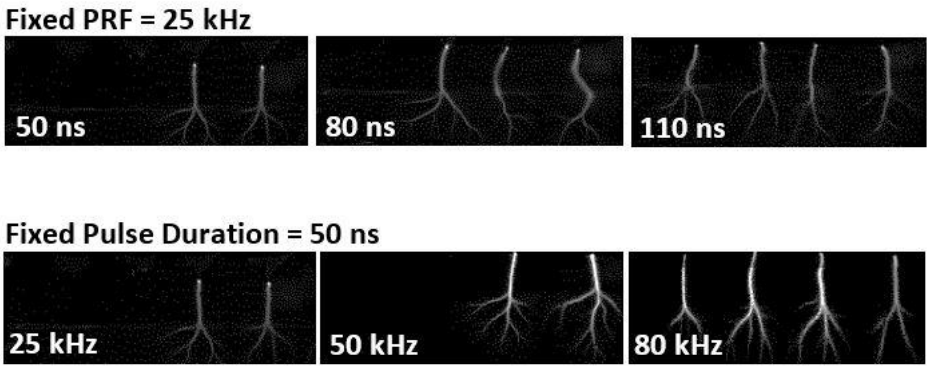

Figure 3.7: Plasma formed in configuration (3) for a range of pulse durations and PRFs.

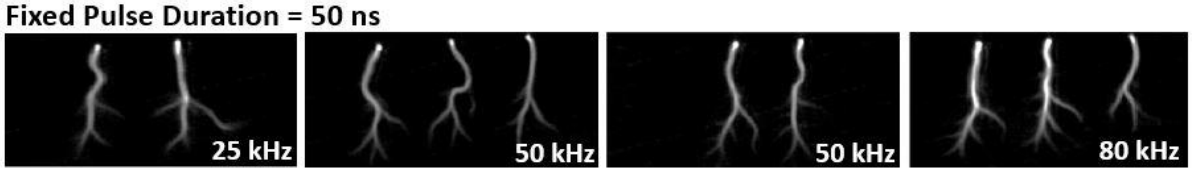

Figure 3.8: High-speed camera images of plasma formed in configuration (4) for a range of pulse durations and PRFs.

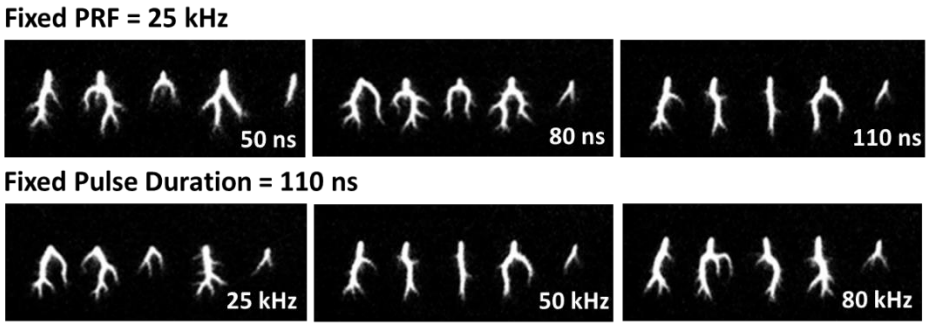

Figure 3.9: ICCD camera images of plasma formed in configuration (4) for a range of pulse durations and PRFs.

Configurations 5 and 6 – Effect of electrode gap

In configurations 5 and 6, the gap between the electrodes was removed but the dielectric barrier was maintained. In the single saw sooth electrode case 5, the plasma filaments are very short in length at low pulse duration (< 50 ns) and become longer and more branched as the pulse duration is increased, as shown in Figure 3.10. The filaments formed in the double sawtooth configuration 6 appear very similar to those formed in configuration 4 and are shown in Figure 3.11. The primary difference is that as the PRF is increased, the plasma filaments increase somewhat in length such that they span nearly the entire extent of the buried electrode. Overall, having no electrode gap increases the intensity of the filaments and causes them to become even more well-defined. The closer proximity of the exposed and buried electrodes possibly enhances the surface electric field between the two electrodes, causing the plasma discharges to improve in structure and brightness. The images in both Figures 3.10 and 3.11 were captured using the ICCD camera, with the gain set to 1, gate delay set to 250 ns and gate width set to 1 ms.

An experimental study by Bayoda et al. [65] investigates the comparison of a single NRP-DBD (generated between electrodes 1 and 2 in Figure 3.12) and a sliding discharge (generated between electrodes 1 and 3 in Figure 3.12), while varying the electrode gap from 40-80 mm. Measurement techniques used to

understand the electrical and mechanical properties of the nanosecond pulsed plasma discharges for the different electrode configurations reveal that the electrode gap does influence the plasma properties. An interesting point to note is that in the plots in Figure 3.12, once the mean surface electric field surpasses the threshold value of 6.5 kV/cm and the sliding discharge is forced, the total energy has the highest value at any given mean surface electric field value for an electrode gap of 60mm. Since the input energy has a great influence on the intensity of the pressure waves generated by discharges [26], an electrode gap of 60mm, rather than a closer proximity of 40mm, would be the optimum gap distance to maximize the actuator's efficiency. While the current work only studies the effect of having an electrode gap versus the effect of having no electrode gap, finding the optimum electrode distance that would give the highest total energy should also be investigated. A sliding discharge configuration could also be considered for large-scale actuators or when the formation of longer plasma filaments is desired. In another similar study by Ndong et al. [66], the effect of varying the electrode gap distance in a typical asymmetric flat electrode NRP-DBD geometry on the discharge characteristics was investigated. It was found that ignition of the discharge was delayed as the electrode gap was increased, due to the decreasing electric field near the active electrode, for the same applied voltage. As shown in Figure 3.13, the discharge current peaks significantly vary for the discharge formation at different electrode gap distances and the optimized gap distance is 1mm since the current amplitude is maximum at that value.

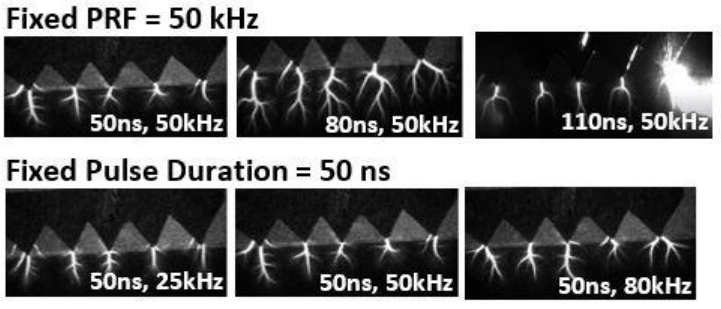

Figure 3.10: Plasma formed in configuration (5) for a range of pulse durations and PRFs.

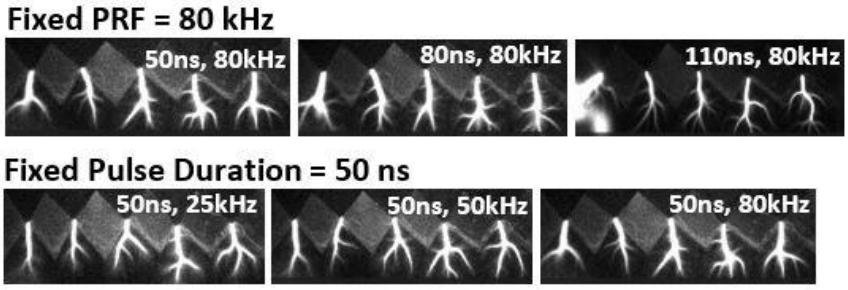

Figure 3.11: Plasma formed in configuration (6) for a range of pulse durations and PRFs.

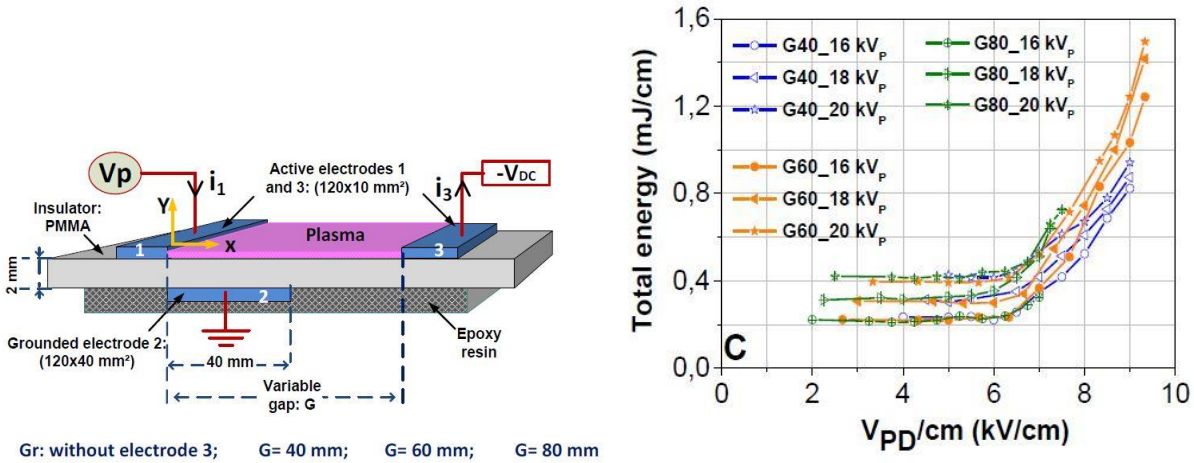

Figure 3.12: Schematic of the actuator geometries (left) and plots of the total energy consumed by the discharge versus the mean surface electric field (right) [65].

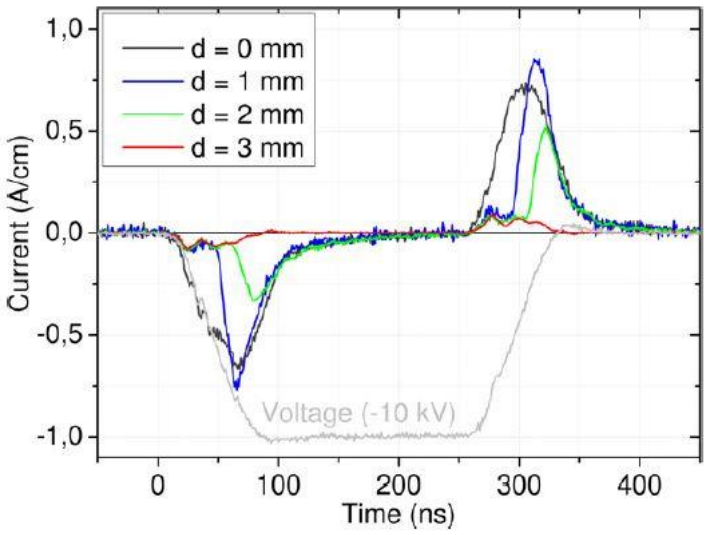

Figure 3.13: Current waveforms for different electrode gaps at -10 kV [66].

Effect of electrode polarity

The effect of the pulse polarity was also investigated and the results of the tests with configurations 3 (single saw tooth, with gap with dielectric barrier), 4 (double saw tooth, with gap with dielectric barrier), 5 (single saw tooth, no gap with dielectric barrier) and 6 (double saw tooth, no gap with dielectric barrier) are shown in Figures 3.14, 3.15, 3.16 and 3.17 respectively. For the double saw tooth configurations 4 and 6, arcing at a pulse duration of 110 ns and 80 kHz does not occur when the negative electrode is exposed, according to Figures 3.15 and 3.17. For the single saw tooth configuration 5, the filaments formed are more branched when the negative electrode is exposed, as seen in Figure 3.16. Dawson et al. [67] conducted a study on the effects of pulse polarity on NRP-DBD actuators and found that negative polarity pulses applied to the exposed electrode of the conventional asymmetric electrode actuator produce pressure waves of higher strength, at a given peak voltage and pulse energy. They further postulated that the coupling of electrical energy to heat energy of the gas near the surface is more efficient when the driven pulses are of negative polarity. This shows some agreement with the current work, where the filaments are more uniform and defined for the single and double saw tooth configurations when the negative electrode is the exposed one,

as mentioned earlier. With filaments that are more structurally sound, the forcing mechanism that affects the flow would also be more efficient. However, for the configurations considered in this work, changing the pulse polarity does not produce as significant a change in the discharge formation as varying the pulse duration and PRF values. The more significant effect on the plasma structure is brought about using a dielectric barrier and the interelectrode distance. The separation of the electrodes by the dielectric barrier seems to form more branched and well-defined filaments. Branching of the discharge filaments occurs regardless of the presence of a gap between the electrodes but appears more pronounced when there is no gap. Therefore, greater focus is directed towards these parameters.

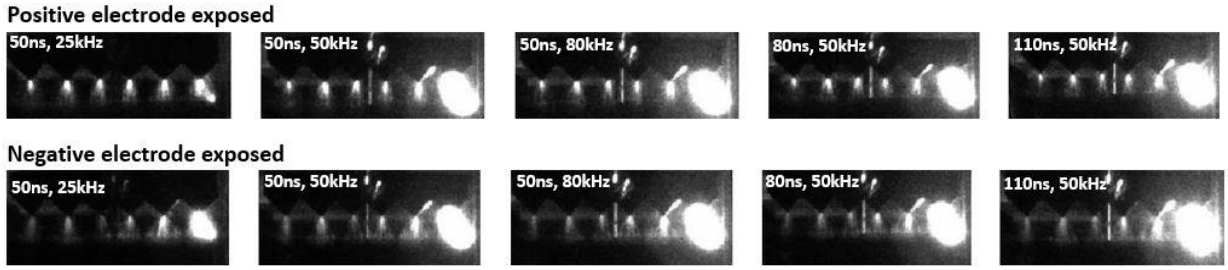

Figure 3.14: Plasma formed in configuration (3) for different polarities of exposed electrode.

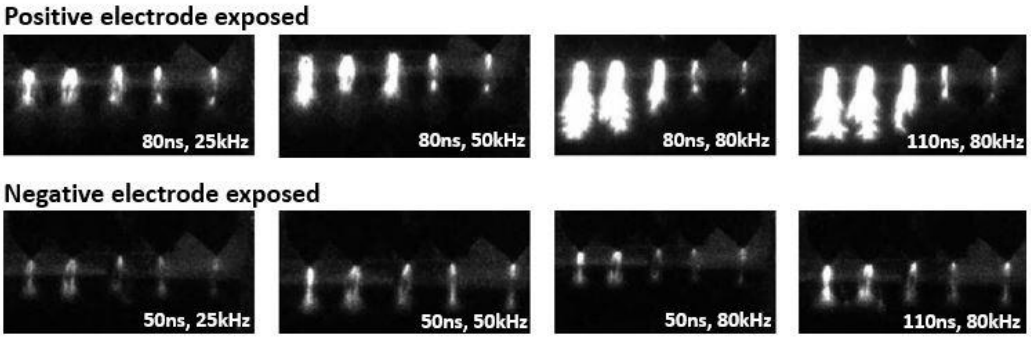

Figure 3.15: Plasma formed in configuration (4) for different polarities of exposed electrode.

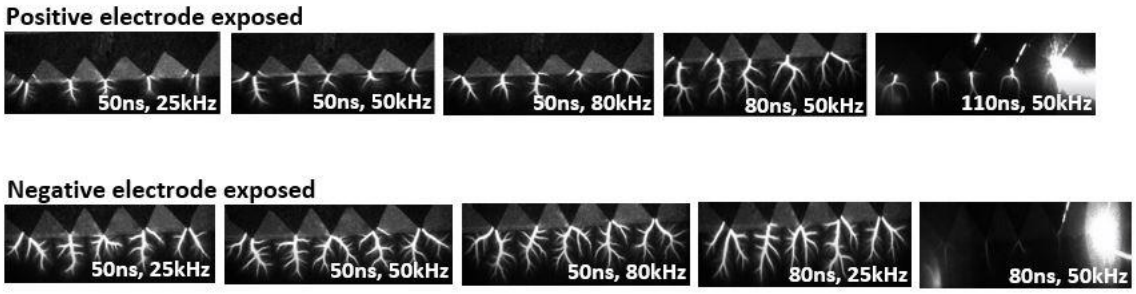

Figure 3.16: Plasma formed in configuration (5) for different polarities of exposed electrode.

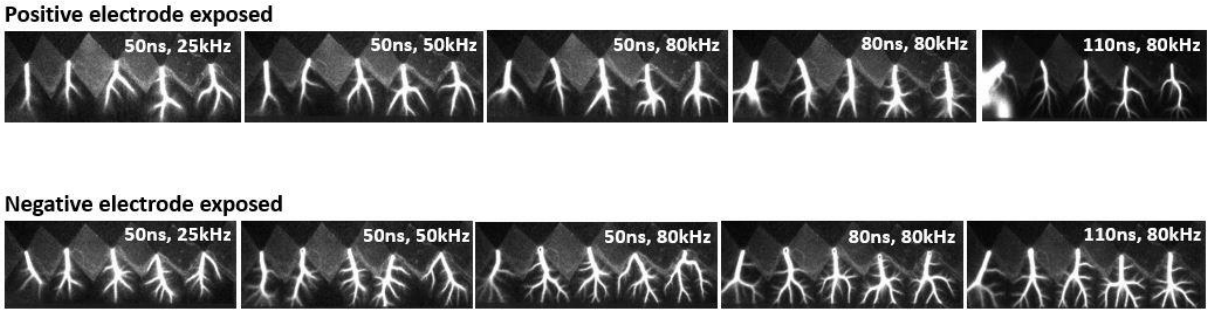

Figure 3.17: Plasma formed in configuration (6) for different polarities of exposed electrode.

3.1.2. Effect of Ambient Pressure

As many supersonic flow applications occur at low ambient pressures, e.g. flight at high altitudes, the effect of low pressures on plasma formation must be investigated. Based on the results presented in the previous section, configuration 6 (double saw tooth with dielectric barrier and no electrode gap) appears to produce the brightest filaments across the electrodes at atmospheric pressure. The "strength" of the filaments, determined by the emission intensity, could be considered as an indicator of relative plasma temperature. Filaments of higher temperature would mean a more pronounced thermal effect and possibly better flow control. Hence, this configuration is tested in ambient pressures below 1 atm to observe how the filament formation is affected. The results are shown in Figure 3.18 and as the pulse durations and PRFs are increased, arcing starts at higher pressures and continues as pressure is lowered. To better understand the effect of a

dielectric barrier and an interelectrode gap distance on NRP SDBD actuators, the single saw tooth configuration without a dielectric barrier separating the electrodes and with a 0.25 in. gap distance between the electrodes, as in configuration 1, is also tested under lower ambient pressures and the results are shown in Figure 3.19. Preliminary experiments at pressures down to 2.7 psi show that as the pressure is lowered, the plasma filaments become more diffuse as expected and the degree of branching decreases. This agrees with a study done by Wu et al. [68] where they found that the discharge mode for an AC-DBD plasma actuator switches from filamentary to glow at a pressure of 0.87 psi. A similar study by Nichols et al. [69] found that a decrease in pressure does not have much of an effect on the electric field close to the exposed electrode but causes the electric field far from the electrode to be close to zero. This could explain why as the pressure is lowered, the plasma filaments become more diffuse as they extend from the exposed to the buried electrode. There is a lack of data on the effect of low pressures on NRP discharges, therefore further study needs to be done in order to truly understand if the effect of lowering the ambient pressure on both AC-DBD and NRP-DBD is similar. From Figure 3.19, as the pulse durations and PRFs are increased, arcing occurs at the higher pressures but disappears as pressure is lowered. The ICCD camera was used to capture the images in Figures 3.18 and 3.19. The gain, gate delay and gate width were set to 1, 250 ns and 1 ms, respectively for the double saw tooth configuration 6. The gain and gate delay were set to 1 and 29ns, respectively for the single saw tooth configuration 1. The gate width for this configuration was varied according to the PRF.

While the focus is on configurations 1 and 6, pressure tests are also conducted for configurations 3 and 4 and the results are included in Figures 3.20 and 3.21. As seen in Figure 3.20 for the single saw tooth configuration 3, as the ambient pressure is reduced below atmospheric pressure, the branching of the filaments decreases, and they become more diffuse. As the ambient pressure is increased above atmospheric pressure, the number of filaments formed decreased and branching increases. For the double saw tooth configuration 4, Figure 3.21 shows that filaments are more diffuse at lower pressures and more branched at higher pressures, like the tests conducted with the

single saw tooth configuration 3, but arcing is more likely to occur at low pressures. For pressures above 1.5 atm, no filaments form. All the images in Figures 3.20 and 3.21 were captured using the SA-Z camera at a frame rate of 50400 fps and a frame exposure time of 1/54842 s for the single saw tooth configuration 3 and a frame rate of 10000 fps and a frame exposure time of 1/119149 s for the double saw tooth configuration 4.

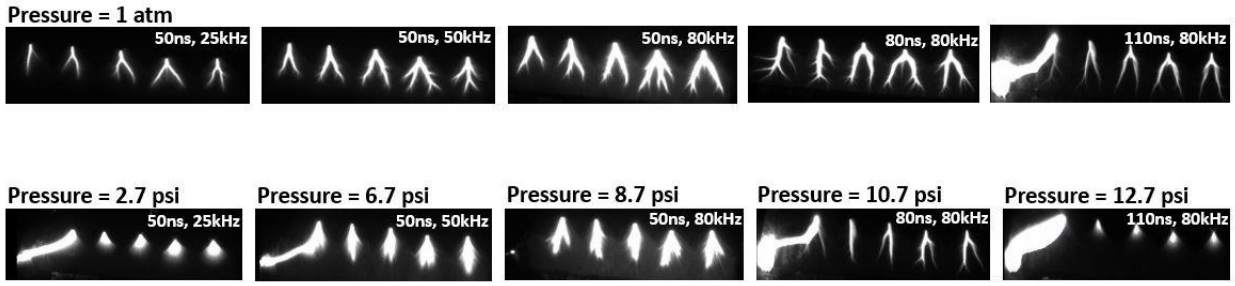

Figure 3.18: Plasma formed in configuration (6) for a range of low pressures.

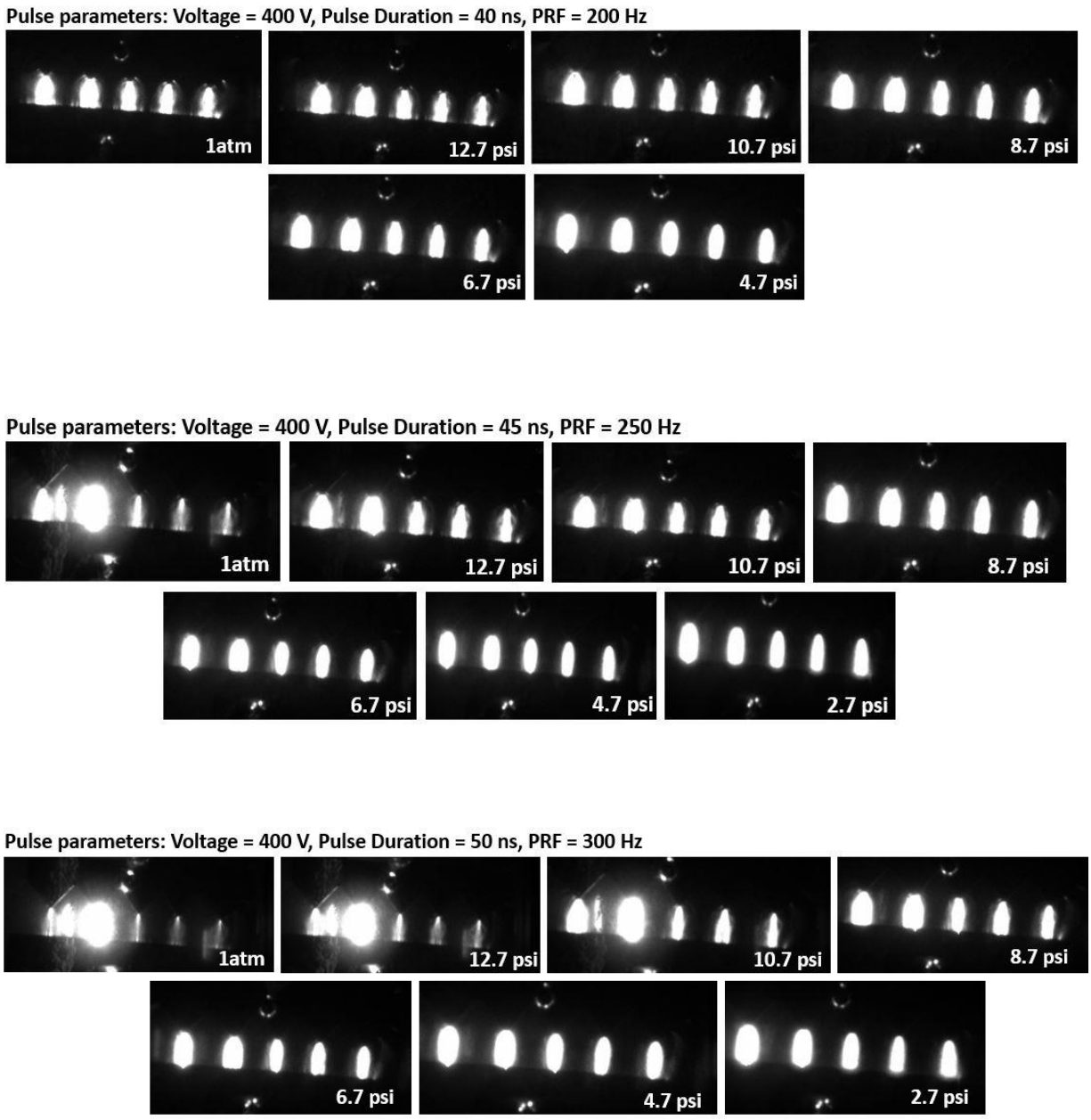

Figure 3.19: Plasma formed in configuration (1) for a range of low pressures.

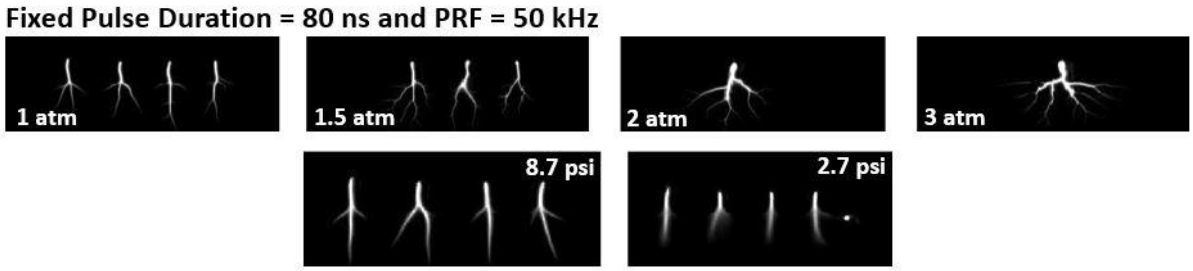

Figure 3.20: Plasma formed in configuration (3) for a range of high and low pressures.

Figure 3.21: Plasma formed in configuration (4) for range of high and low pressures.

Mitigation of arcing issue

A major challenge is the arcing of the filaments formed on the NRP SDBD actuators. At atmospheric pressure, increasing the pulse parameters beyond certain values for the different configurations causes arcing. Moreover, arcing seems to be induced by the low ambient pressures for the double saw tooth configuration (6) but occurs at higher ambient pressures for the single saw tooth configuration (1). Nichols et al. [68] postulated that power consumption by the actuator increases as the pressure is decreased because more power is used to generate the plasma rather than to accelerate it. Their experimental results showed that there was a coincidence between the location of peak charge buildup and location of peak surface potential, leading them to conclude that the deposition of charge is the main mechanism for increasing the potential on the surface of the dielectric, rather than the potential increase by polarization effects due to the actuator.

Assuming this same phenomenon occurs with NRP discharges, the excess charge deposition at lower pressures could be the reason for an increased chance of arcing.

Table-top tests with the double saw tooth configuration (1) have provided some understanding of the arcing phenomenon. Forcing the plasma discharges multiple times induces arcing. Tests conducted, where the pulse parameters can be increased to a pulse duration of 110 ns and PRF of 50 kHz before arcing occurs, see arcing occurring at the lower pulse durations and PRFs when the plasma discharges are made to form multiple times. Arcing induced by higher pulse durations and PRFs can trigger arcing when the pulse parameters are lowered. Once the arcing path is created at higher pulse parameters, the issue continues even when the pulse parameters are lowered back to the values at which arcing initially did not occur. A noteworthy phenomenon is that when arcing at lower pulse parameters (e.g. pulse duration = 50ns, PRF = 25 kHz and pulse duration 80 ns, PRF = 25 kHz where arcing did not occur initially) is triggered by the arcing at higher pulse parameters, the issue goes away after the first few pulses at the lower pulse parameters. However, this was not a consistent result.

A more homogenous filament structure is desired since the uniformity of the plasma would make flow control more stable and predictable. Methods for mitigating the arcing have been explored. These include attaching of one of the electrode connection wires from the back of the acrylic, using high-voltage resistors to limit the current to the electrodes and adding more layers of dielectric tape between the electrodes. These methods are discussed below. Each method shows some improvement in reducing the arcing, but none completely resolve the issue. A combination of these methods, in addition to more precise fabrication of the electrodes, will be considered for future tests.

Attachment of electrode connection wires from the back of the acrylic

In order to increase the distance between the connection wires and to reduce the likelihood of arcing from one wire to the other, the wire connection to the buried electrode is done from the back of the acrylic plate, as shown in Figure 3.22.

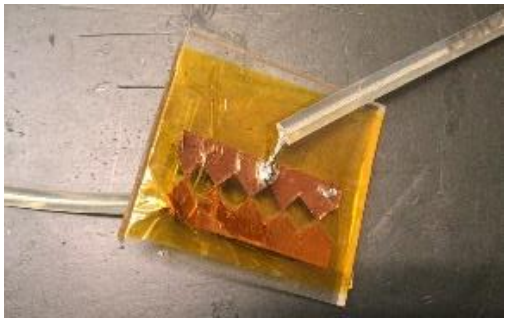

Figure 3.22: Double saw tooth electrode configuration DBD actuator with one connection wire attached from the back of the acrylic.

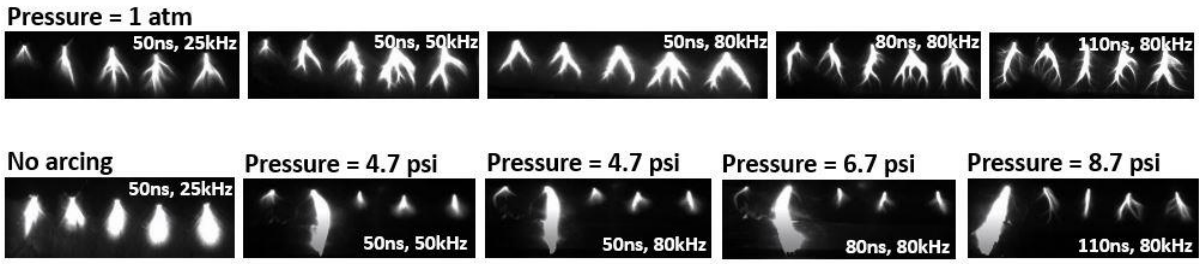

Figure 3.23: Plasma formed in configuration (6) as shown in Figure 3.17 for a low range of pressures.

Comparing the results shown in Figure 3.23 to the results from Figure 3.18, arcing now begins at lower pressure values as the pulse durations and PRFs are increased. Hence, attaching the connection wire to the buried electrode from the back of the acrylic does help delay arcing.

Limiting the current to the electrodes using high-voltage resistors

To understand if the arcing is caused by a current influx to the electrodes, high-voltage resistors are attached to the electrodes to limit the current. The single saw tooth electrode configuration (1) without the dielectric is used for this series of tests and these are conducted at atmospheric pressure. As shown in the schematic in Figure 3.24, a 1000 ohm high-voltage resistor (RT818A102K) is attached to the saw tooth electrode.

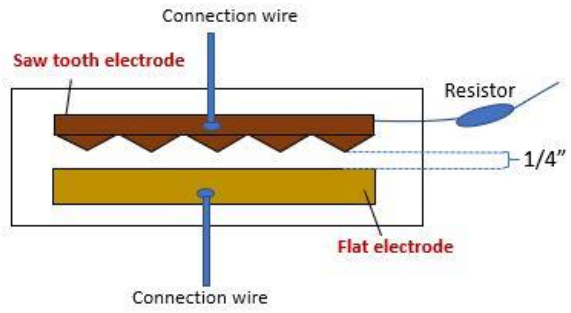

Figure 3.24: Schematic of single saw tooth electrode configuration (1) with a high-voltage resistor attached to the saw tooth electrode.

The starting pulse parameters are a pulse voltage of 400 V, pulse duration of 40 ns and PRF of 200 Hz. From Figure 3.3, we know arcing for configuration (1) occurs for pulse durations above 30 ns and PRFs above 250 Hz and hence arcing is expected at a pulse duration of 40 ns and a PRF of 200 Hz. Arcing occurs at the left most saw tooth of the configuration (1). Upon attaching a resistor to the saw tooth electrode, arcing stops and uniform dome shaped filaments are formed. As the pulse duration is increased to 50 ns, keeping the PRF constant at 200 Hz, the filaments become brighter but remain uniform. Increasing the pulse duration to 60 ns, arcing occurs once again at the left most saw tooth. An additional resistor is attached in series to the initial resistor and uniform filaments form. As the pulse duration is increased to 70 ns, the filaments remain uniform while increased slightly in brightness. Increasing the pulse duration from 80-110 ns, in intervals of 10 ns, still forms uniform filaments with the brightness increasing much lesser than before. The results

for the tests at a pulse voltage of 400 V and PRF of 200 Hz and with the attachment of two resistors are shown in Figure 3.25. The PRF is then increased to 250 Hz and the pulse duration is reduced back to 40 ns. Increasing the pulse duration from 50-90 ns, in intervals of 10 ns and keeping the PRF at a constant of 250 Hz, continues to form uniform filaments. At 100 ns and 110 ns, faint arcing occurs. The results for the tests at a pulse voltage of 400 V and PRF of 250 Hz and with the attachment of two resistors are shown in Figure 3.26. Increasing the PRF to 300 Hz and varying the pulse duration from 40-70 ns, in intervals of 10 ns, forms uniform filaments and arcing occurs at a pulse duration of 80 ns. A third resistor is added to the first two in series and arcing stops. The results for the tests at a pulse voltage of 400 V and a PRF of 300 Hz and with the attachment of two resistors are shown in Figure 3.27.

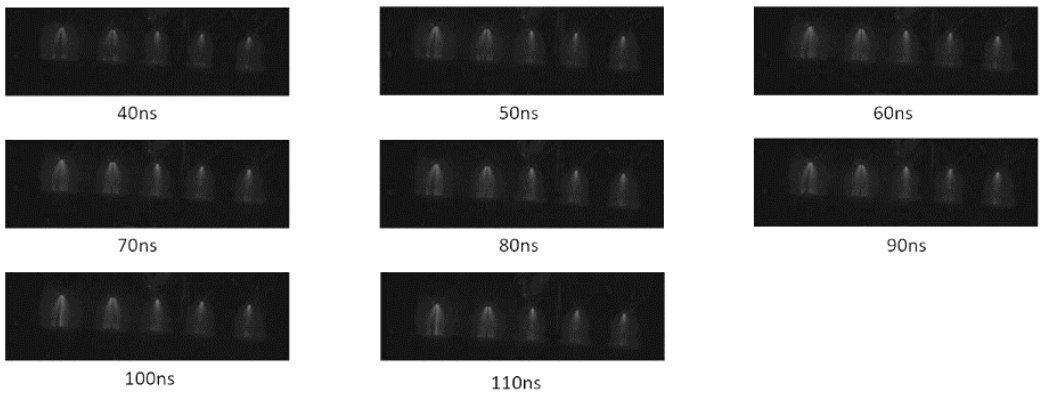

Figure 3.25: Plasma formed in configuration (1) (with 2 resistors attached to the saw tooth electrode) at a pulse voltage of 400V and PRF of 200 Hz.

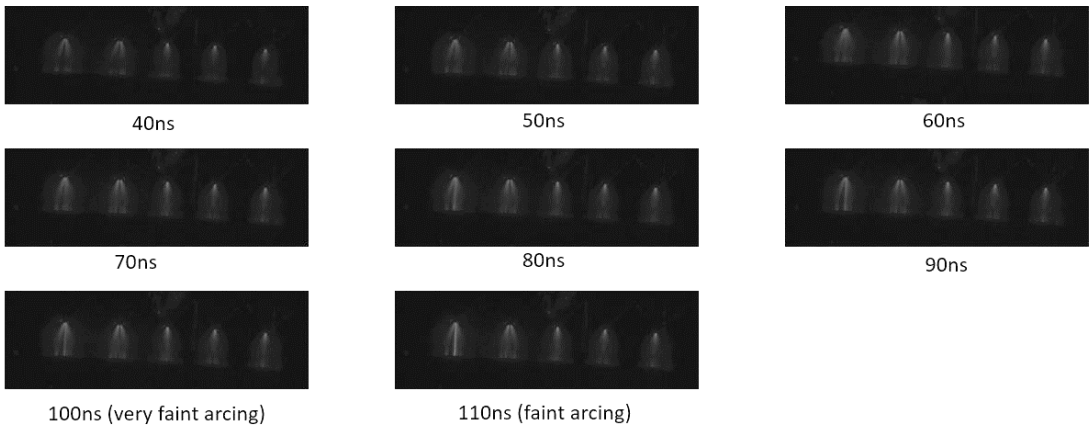

Figure 3.26: Plasma formed in configuration (1) (with 2 resistors attached to the saw tooth electrode) at a pulse voltage of 400 V and PRF of 250 Hz.

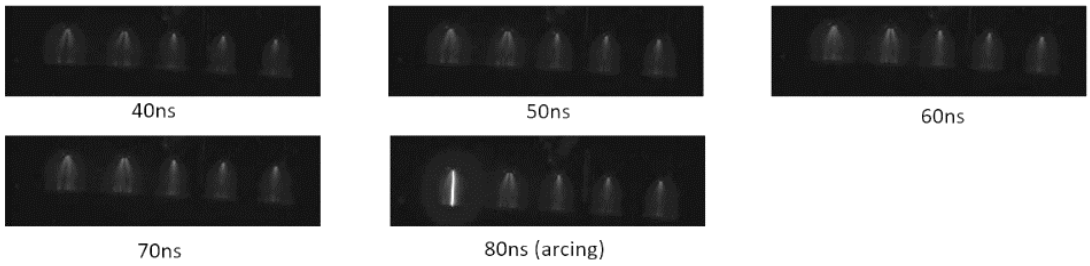

Figure 3.27: Plasma formed in configuration (1) (with 2 resistors attached to the saw tooth electrode) at a pulse voltage of 400 V and PRF of 300 Hz.

Addition of high-voltage resistors can curb the arcing, but this is not a feasible solution since the number of resistors required varies with the pulse parameters. There is no tangible correlation between the pulse parameters and the number of resistors required to prevent arcing. A possible extension of this method could be to make the resistance a variable one, whereby the resistance value can be easily changed whenever arcing occurs for a set of pulse parameters. However, this would also not be a permanent fix to the arcing issue and involves a lot of uncertainty.

Adding more layers of dielectric tape between the electrodes

The dielectric barrier material chosen while fabricating the actuator plays a huge role in determining the efficiency and the durability of the device [70]. The initial actuators used in the current work had two layers of 0.0025 in. thick Kapton tape as the dielectric barrier separating the electrodes. When an additional layer of dielectric tape is added, arcing is delayed at the higher pulse durations and PRFs. This is expected because with an increased thickness in the dielectric barrier, there is a greater spread of the electric field lines on the surface, which in turn sees a decrease in the current density. With a lower current density, the likelihood of arcing occurring is reduced. In a study by Thomas et al. [64], in the field of AC-DBD actuators, in addition to increasing the thickness of the dielectric barrier, it was found that using dielectric material of lower dielectric constant could considerably increase the maximum voltage used before the point of saturation, that being the formation of streamer filaments. The effective capacitance of the actuator decreases when a material of lower dielectric constant is used. There is a decrease in the local concentration of electric field lines and hence, the current density. This would allow the actuator to operate at higher voltages without the formation of streamers. Their experimental results showed that the use of dielectric barrier materials of low dielectric constant, high dielectric strength and increased thickness saw an increase by an order of magnitude, in the body force produced by the plasma discharges, compared to the use of 0.006 in. thick Kapton. There have been many other such studies on the dielectric material choice for AC-DBD actuators, but studies of a similar extent have not been conducted for NRP-DBD actuators [71]. Correale et al. [70] conducted a study on characterizing the energy deposition of NRP-DBD actuators based on the properties and geometry of the dielectric barrier material. They found that the energy deposition within the volume of the discharge has a strong dependence on both the type and the thickness of the dielectric material used. In the tests using Kapton as the dielectric material, they observed that as the thickness of the barrier is increased, the energy release to the air inside the discharge volume decreases. This is possibly because a larger separation between the electrodes would mean a lower electric field created between them. This would in turn lead to a weaker discharge formation and hence, a smaller energy deposition. Moreover, they

postulated that thinner barriers would be more reliable since more layers of Kapton tape would mean more layers of silicon-based adhesive, which would introduce more impurities within the barrier. Therefore, for NRP-DBD actuators, increasing the thickness of the dielectric barrier by adding more layers might be detrimental to the efficiency since the impact of the main forcing mechanism is reduced. Correale et al. concluded that using a material that can satisfy as many of these properties – high dielectric strength (to minimize the thickness of the material), low volumetric resistivity (to maximize the extent of the plasma region), heat capacitance and thermal conductivity coefficient (to minimize the heat dissipation within the actuator itself), would be best to ensure maximum efficiency of NRP-DBD actuators. In a study by Rodrigues et al. [72], measurements of the power generated as heat from actuators using different dielectric materials was taken and they too concluded that the dielectric material choice affects the heat generation.

In addition to the thickness and the dielectric property factors, when considering the dielectric barrier material, the strength and quality should also be accounted for. Three layers of Kapton polyimide film of thickness 0.002 in. is a common option for the dielectric barrier on SDBD plasma actuators used for flow control. However, there have been many recent studies looking into building DBD plasma actuators using materials of better durability when in contact with plasma. Houser and co-workers studied the methods of manufacturing DBD plasma actuators and came up with a high precision manufacturing process using microfabrication techniques [73]. In their study, they found tungsten to be a more robust material for the electrodes compared to copper and used degradation-resistant glass as the dielectric barrier. Aging of the dielectric has also been found to influence the structure, as well as the electrical characteristics of NRP plasma discharges [74]. Ndong and co-workers [74] investigated this effect by aging a typical asymmetric flat electrode geometry actuator using a positive 10 kV voltage pulse continuously applied to the exposed electrode, while keeping the buried electrode grounded, for a duration of 15 minutes, at a pulse duration and pulse frequency of 250 ns and 1kHz, respectively.

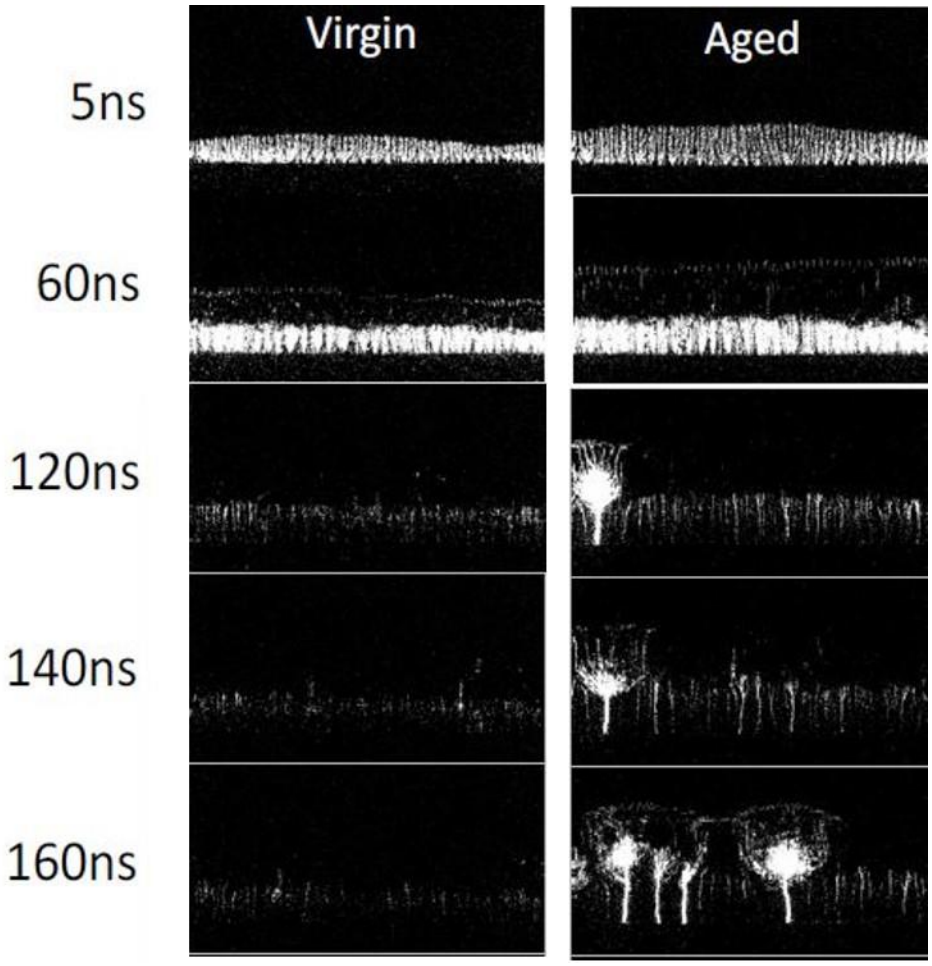

Figure 3.28: Development of plasma discharges over time [74]

The ICCD images in Figure 3.28 show part of the discharge development at different points in time, with the gate width on the camera set to 5 ns. The voltage plateau at 10 kV lasts from 120 to 240 ns, and an example of the filaments formed from at 120 ns, 140 ns and 160 ns are shown. During this plateau, for the aged actuator, there are distinct large filaments which are much brighter than the other smaller and dimmer ones. Ndong et al. postulate that the shift in the positions of the large filaments could mean a non-localized origin of the plasma discharges, which in turn, could be due to geometrical issues along the edge of the exposed electrode. They further explain that these discharges could be induced by an augmentation of the local electric field due to the charges that remain on the dielectric surface and conclude that the aging of an actuator would favor high concentrations of these excess charges. This would explain the arcing issue in

the current work. Arcing is less likely to occur for new actuators but upon using the actuator for multiple tests, especially once the arc has been formed, arcing occurs much more easily. Moreover, Ndong et al. mention that forcing these NRP discharges at high frequency would increase the rate of aging and cause the degradation of the surface to hold on to more charge. Therefore, to entirely avoid arcing at high pulse durations and PRFs, it may be best to replace the entire actuator or at least the dielectric barrier with a new one for every test. Moreover, monitoring the degradation of the dielectric material by measurement of the electrical parameters, power consumption and effective capacitance for instance [75], could be an additional precaution to ensuring that the efficiency of the DBD actuator is not compromised by the deficiency of the dielectric barrier.

Figure 3.29: Double saw tooth configuration (6) DBD actuator.

The issue of arcing seems to resolve itself when the length of the actuator is increased to include a greater number of saw teeth, as shown in the test section in Figure 3.29. This test section is placed

in a large section supersonic tunnel to do a preliminary study of the effect of the plasma discharges on the shock waves generated, using background-oriented schlieren. Both the connection wires are soldered onto the electrodes from the back and the surface is made as flush as possible to prevent any arcing that might be induced by sharp edges. Furthermore, only one layer of Kapton dielectric tape of thickness 0.0025" is used as the dielectric barrier between the electrodes. As the pulse duration is increased from 50-110 ns and the PRF is increased from 25-80 kHz, at a pulse voltage of 400 V and a train of 200 pulses, no arcing occurs. To investigate if the number of pulses might influence the arcing, setting the pulse duration at 50 ns and the PRF at 25 kHz, the pulse train is increased up until 1000 pulses, whereby arcing occurs. Therefore, increasing the number of saw teeth and having both wire connections to the electrodes from the back would be a feasible solution for future testing purposes. In addition to this, machining the electrodes to ensure precision in the alignment of the saw teeth would be helpful in resolving the arcing issue.

Actuator voltage and current measurements for this test section were taken using an Agilent Technologies Infinium DSO9104A oscilloscope. Some samples of the V-I plots at different pulse parameters are shown in Figure 3.30. The actuator voltage ranges around 7-8 kV and the actuator current ranges around 30-40 Amperes. As the pulse parameters are increased, there is more jitter during the voltage falling as well as in the current after the peaks. Comparing the V-I plots for the smaller optimized DBD actuator and the larger one on the test section at a pulse duration of 110 ns and PRF of 50 kHz, as shown in Figure 3.31, the peak voltage is almost twice as much for the smaller actuator. Having a larger DBD actuator with many more saw teeth could mean that a lower voltage is required for the plasma to breakdown. With a lower breakdown voltage, the actuator power consumption to drive the plasma discharges would be lower. The current trace on the left for the smaller DBD actuator sees additional peaking and an uneven fall after the duration of pulse

discharge. This could be evidence that there may be geometrical issues or that the dielectric barrier needs to be changed since it may be holding on to the excess charges from the plasma discharge due to aging from multiple tests, causing the current trace to be so uneven. The current trace for the larger DBD on the right is much less chaotic and this could be attributed to the dielectric barrier being relatively new.

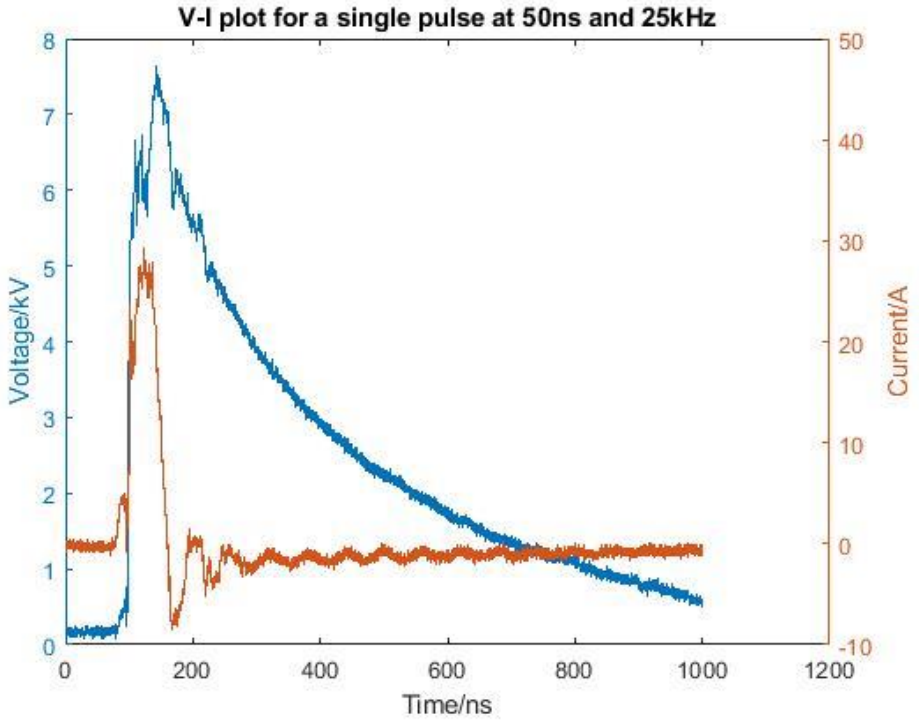

Figure 3.30: V-I plots for the test section of a single plasma pulse at different pulse parameters.

Figure 3.30 continued

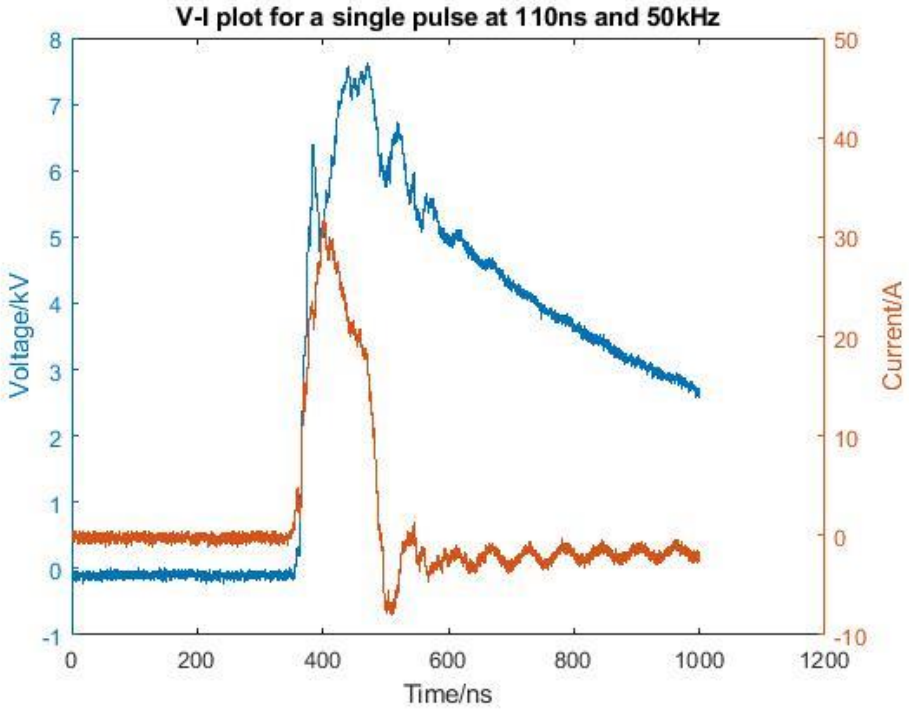

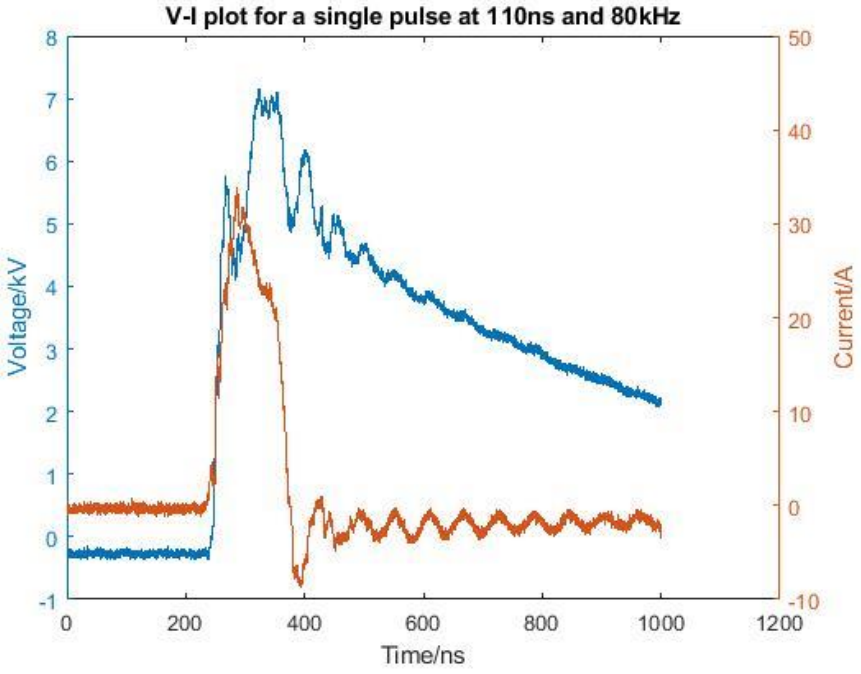

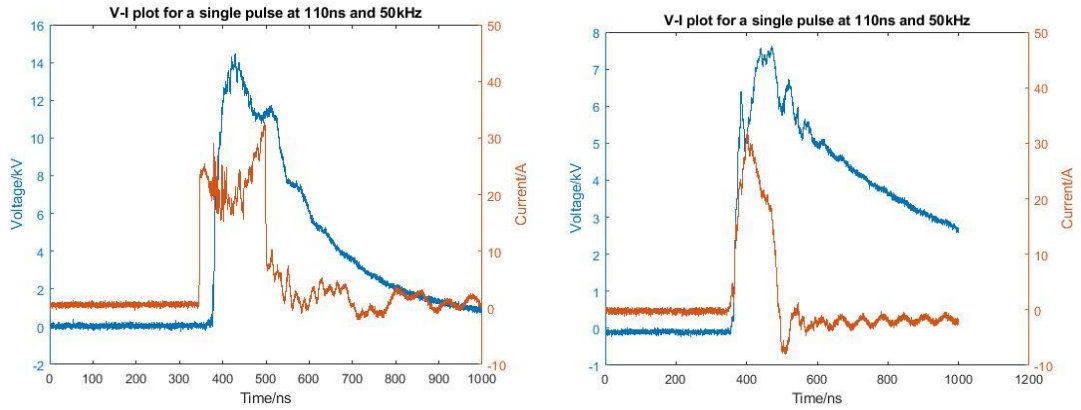

Figure 3.31: V-I plots for a smaller optimized configuration DBD actuator (left) and for the large-scale actuator on the test section (right) of a single pulse at a pulse duration of 110 ns and PRF of 50 kHz.

3.2 Plasma Temperature and Induced Flow

The brightness of the filaments may be an indication of the temperature of the filaments produced. A diffuse discharge structure is visually less bright than the constricted filamentary structure, which could mean that the plasma is at a lower temperature. The thermal effect of the discharge on the surrounding air and thus the induced flow would also be different. Hence, measurements of the plasma character are important to characterize the effect of electrode geometry, pulse parameters and pressure on the temperature perturbation of the discharge. The OES system described in Chapter 2 has been used to obtain preliminary temperature measurements using electrode configuration 6 (double saw tooth with dielectric and no gap) with different values of pulse duration and PRF. The spectrometer slit width is 20 μm and the gain is set to 25 on the ICCD camera. The ICCD camera gate was 150 ns to capture all emission during a single discharge, and 200 pulses are accumulated for each experimental spectrum. Theoretical fits for the spectra are obtained using Specair software to calculate an average (in time and space) temperature for a single filament. A 1800 g/mm grating is used to obtain temperature fits of higher accuracy for the

vibrational temperatures while a 2400 g/mm grating is used to obtain temperature fits of higher resolution for the rotational temperatures.

Experimental and theoretical spectra are shown in Figures 3.32 and 3.33, using the 1800 g/mm and 2400 g/mm gratings, respectively. The pulse parameters that have been chosen are those for which no arcing is observed, according to the prior tests done using configuration 6. Qualitatively, the fit between experimental and theoretical spectra appears to significantly improve with higher PRF, likely due to the improvement in the signal-to-noise ratio. The rotational and vibrational temperatures obtained for pulse durations of 50, 80, and 110 ns and PRFs of 25, 50, and 80 kHz are given in Table 3.1. For the two lower PRF values, the rotational temperature rise is somewhat consistent with the results of Takashima et al. [62] for a 10 kHz discharge (~380-450 K). The temperature rise is much higher (~620 K) for a PRF of 80 kHz. The vibrational temperature is quite high, on the order of 5000 K, and does not vary significantly with changing PRF. The effect of pulse duration is not clear from these limited measurements. While these measurements confirm a rapid (within the first 150 ns) increase in temperature due to the plasma filament, there is some notable inconsistency in the temperature values and the theoretical spectral fits need to be significantly improved. From Figures 3.32 and 3.33, it is evident that for lower PRF values of 25 kHz and 50 kHz, the fits are generally poor. There should be a more curved structure throughout, with peaks and falls, for the rotational temperature fits, like for the 80 kHz PRF cases. However, in the cases of the 25 kHz PRF and the 50 kHz PRF fits, the experimental plots are flat and show an intensity of 0 for some wavelengths immediately after the vibrational temperature peaks, before picking up some intensity again. This could be due to the intensity of signal picked up from the plasma emission being too low to be captured at lower PRF values. Higher PRF values for the higher pulse durations were not studied due to influence of arcing, which may then not provide fully accurate data for the temperatures of the plasma filaments. The arrangement of the optical system needs to be very precise in order to have a strong signal and to get maximum emission from the plasma. Unfortunately, even with precision of the optical system, if the plasma

emission is not strong enough to be captured, the signal is going to be poor and hence the fits are not going to be good.

The results from a similar study done on an AC-DBD by Chatelain et al. [76] could be compared to shed some light on this. OES is used to get temperature measurements for a linear and a serrated DBD actuator, and comparison of the results showed that the gas temperature is much higher at each of the tips of the serrated electrode. The rotational temperature determined from the N_2 spectra for the serrated electrode geometry is 520 (± 5) K. For the linear electrode geometry, the rotational temperature is 445 (± 5) K. These were measurements made at a peak pulse voltage of 10 kV and a PRF of 1 kHz. Given that much higher PRF values are tested in this study and that NRP discharges are known to produce much more rapid and localized heating compared to AC discharges, the rotational temperature should be around the same range, if not higher. Hence, the rotational temperature of 911 K for the 80 kHz PRF case in Table 3.1 is probably much more reliable than the temperatures for the 25 kHz and the 50 kHz cases, confirming that increasing the PRF would result in improved temperature measurements. Furthermore, using the 2400 g/mm grating for all tests would help improve the spectral resolution, even if it means a compromising the wavelength coverage. Better fits can also likely be obtained by increasing the number of accumulations; for example, the two prior OES studies used “several hundred” [62] to 2000 accumulations [49].

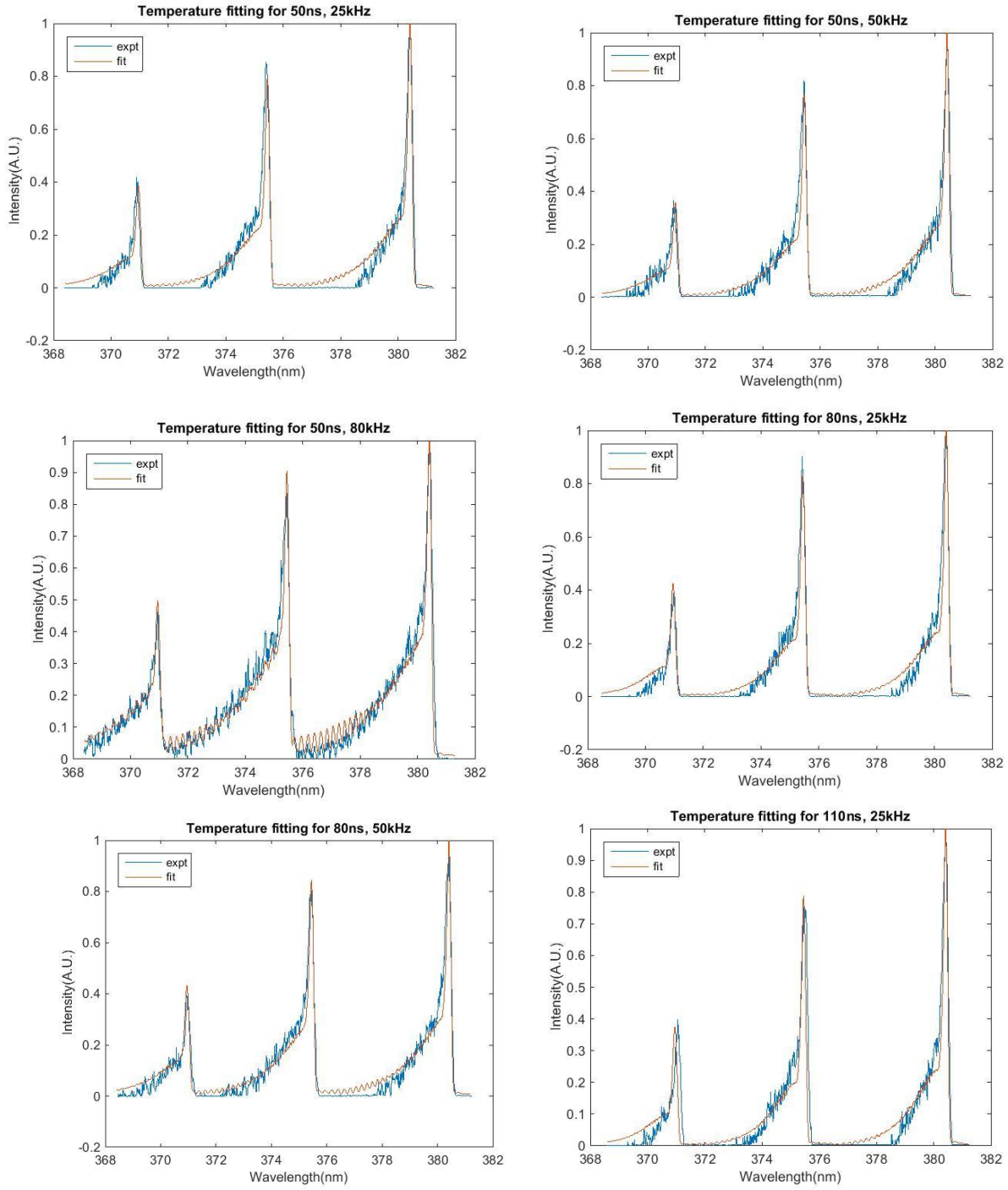

Figure 3.32: Experimental and theoretical spectra of the second positive system of nitrogen for a single plasma filament using the 1800 g/mm grating. The experimental spectra are time-averaged (150 ns gate) and are obtained using 200 accumulations.

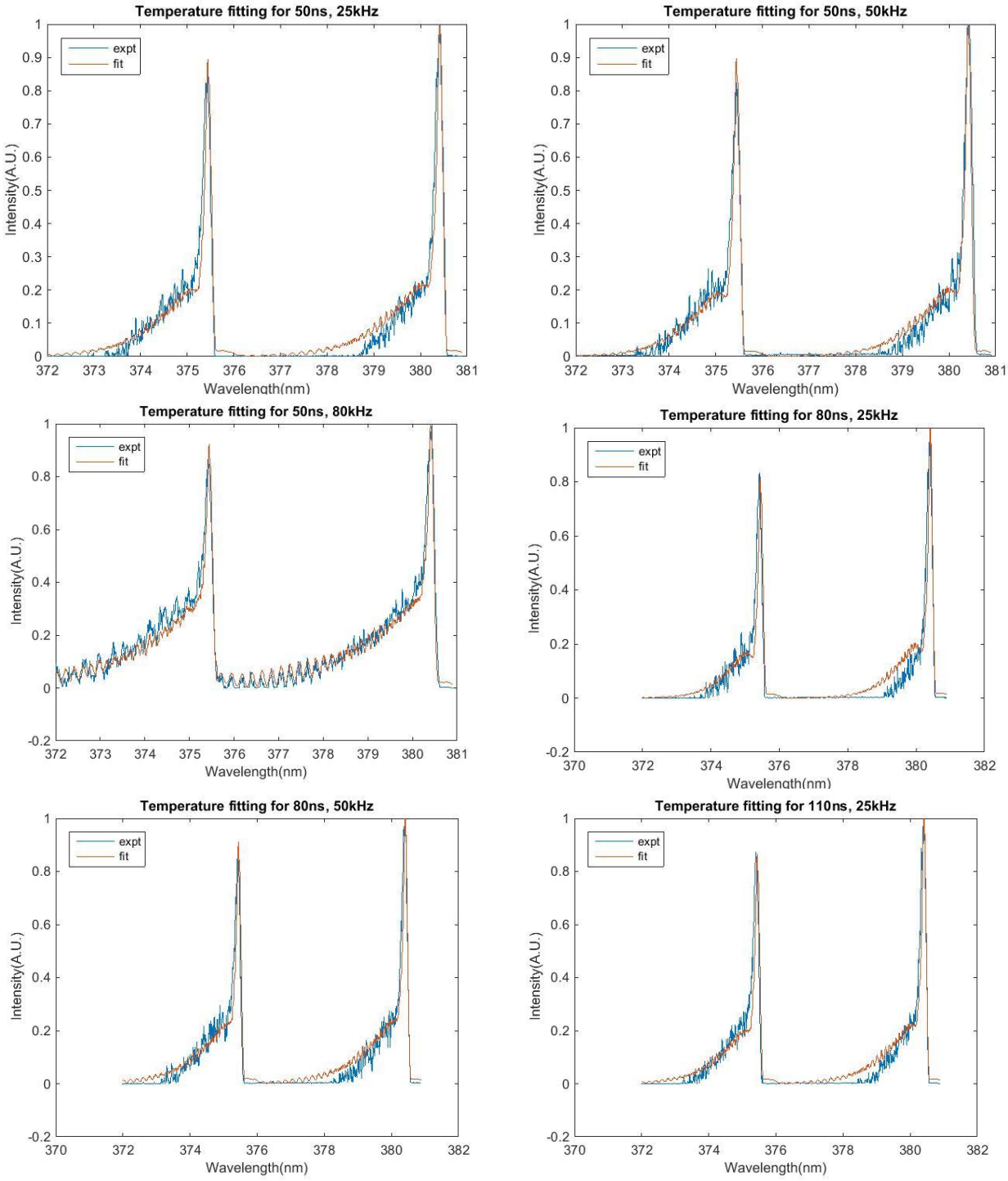

Figure 3.33: Experimental and theoretical spectra of the second positive system of nitrogen for a single plasma filament using the 2400 g/mm grating. The experimental spectra are time-averaged (150 ns gate) and are obtained using 200 accumulations.

Table 3.1: Plasma rotational and vibrational temperatures obtained using OES for a range of pulse parameters.

Grating	Temperature	Pulse parameters					
		50ns, 25kHz	50ns, 50kHz	50ns, 80kHz	80ns, 25kHz	80ns, 50kHz	110ns, 25kHz
1800 g/mm	$T_{vibrational}$/K	5143	4801	5915	5674	5616	5050
2400 g/mm	$T_{rotational}$/K	398	342	911	304	486	421

In addition to OES measurements, the schlieren setup discussed in Chapter 2 is used to visualize the shockwaves and heated gas flow induced by the plasma, as shown in Figure 3.34. The optimal actuator geometry (configuration 6: double saw tooth, no gap with dielectric barrier), as determined from the tests described in Section 3.1, is used to generate the plasma discharges. As the pulse repetition frequency increases, the frequency of the shock waves also increases as expected. The production of these pressure waves is another indicator of rapid heating by the plasma filaments and has been observed in numerous prior studies. As the PRF and pulse duration increase, the volume of heated gas near the surface grows larger; prior work [50] suggests this is primarily an effect of the higher PRF and not of the longer pulse duration.

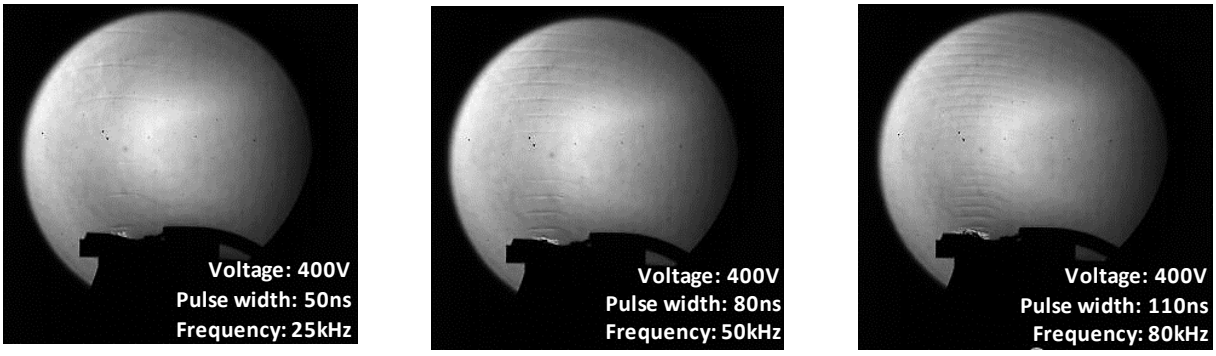

Figure 3.34: Schlieren imaging of induced flow field by plasma in quiescent air at different pulse parameters.

3.3 Plasma Structure in High-Speed Flow

The effect of supersonic flow on the structure of the filamentary discharge is studied by placing the same actuator (configuration 6) on the ramp model in the supersonic wind tunnel as described in Chapter 2.

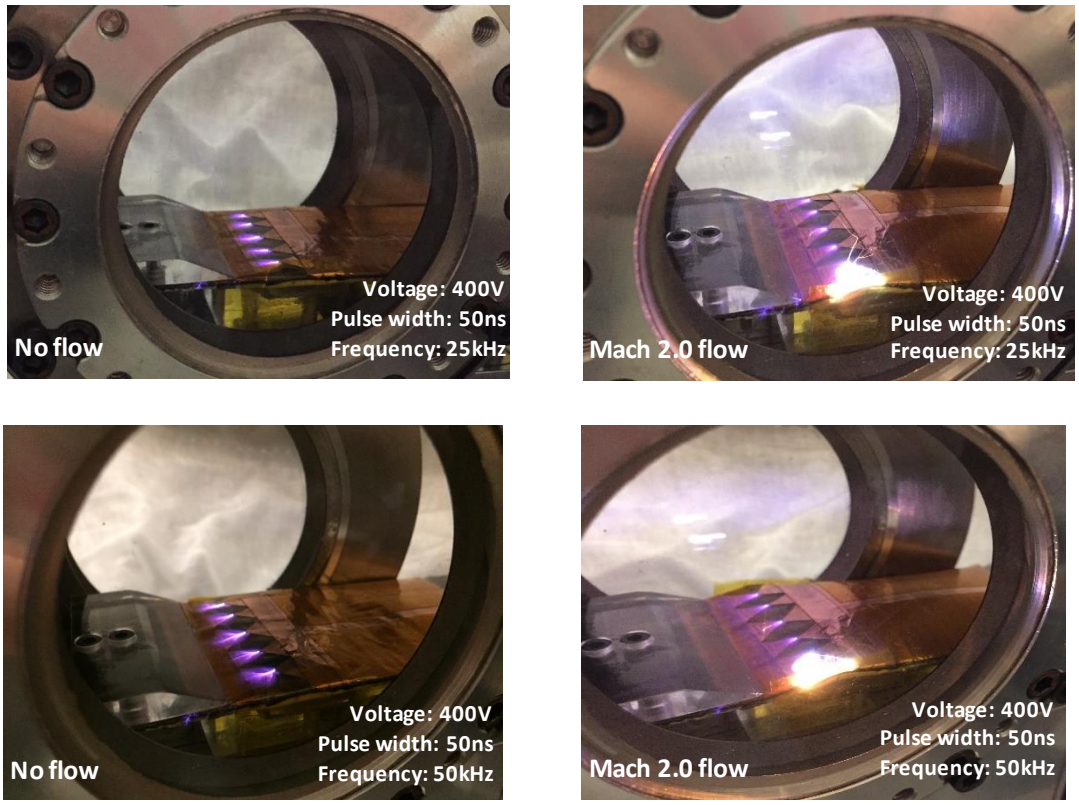

Figure 3.35: Plasma discharges using configuration 6 (double saw tooth, no gap with dielectric barrier) in Mach 2.0 supersonic flow.

As shown in Figure 3.35, the filamentary discharges become much shorter, less branched and appear to glow just at the points of contact of the saw tooth electrodes. Arcing at one saw tooth on one of the sides is once again an issue when the plasma discharges form in supersonic flow. To understand if this issue is purely due to the flow or is also caused by any inaccuracies in the electrode geometry, the saw teeth at the sides are disregarded and only the middle three saw teeth

are considered. According to Figure 3.36, this modification does help to mitigate the arcing issue slightly but increasing the pulse duration or the PRF once again causes arcing.

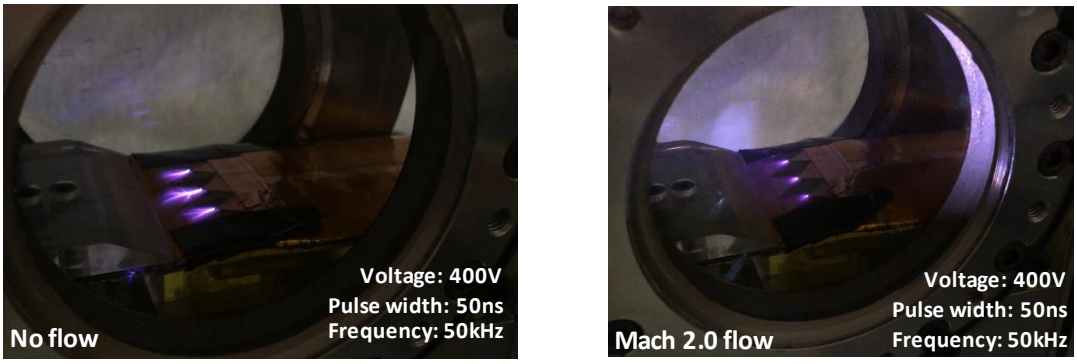

Figure 3.36: Plasma discharges using a modified version of configuration 6 (double saw tooth, no gap with dielectric) in Mach 2.0 supersonic flow.

Furthermore, the schlieren images captured to understand the effect of the plasma discharges on the shock wave caused by the ramp do not show the relevant information. Due to geometrical inaccuracies, undesirable shock waves are produced by various points of the model, affecting the shock wave at the base of the ramp. The initial model had some chipped off edges and these edges were made to be smooth and flushed using Kapton tape and regular adhesive tape. Even though the surface of the actuator seemed to be smooth to the naked eye, there is still some roughness that causes the formation of several undesirable shock waves. Also, the tape used was not strong enough to hold down the actuators to the acrylic and kept lifting whenever the flow in the tunnel was turned on. Therefore, an entirely new model that is much more robust and machined to high precision needs to be built in order to avoid these unnecessary effects and to purely understand how the shock wave at the ramp is affected by the plasma actuator.

CHAPTER 4. CONCLUSION AND FUTURE WORK

Conclusion

The investigations conducted to look at the effect of various other parameters (electrode geometry, dielectric, interelectrode gap, electrode polarity and ambient pressure), apart from the pulse parameters, on the NRP plasma discharges revealed some new conclusions pertaining to the characteristics of these discharges. From past literature, we know that the transition of the plasma mode from a uniform to a filamentary discharge can be influenced by modifying the pulse voltage and pulse repetition frequency. To gain a better understanding of the effect of the pulse duration, the study prior to the current work investigated the characteristics of NRP discharges on a conventional asymmetric flat electrode DBD actuator. It was found that an increased pulse duration can constrict the plasma to a filamentary discharge, even if the frequencies were kept low and on the order of 1 kHz. In addition to being able to vary the physical structure of the plasma discharges by changing the pulse parameters, there was a further curiosity towards having a greater authority over producing controlled and localized filaments. This led to investigating other electrode geometries and it was found that the saw tooth/serrated electrode allowed for better control of the location of the filaments as well as increased intensity of the filaments.

With the understanding that NRP discharges use thermal perturbations as the control mechanism to induce flow, there was a need to investigate the formation of filaments that could produce the required rapid localized heating. An initial assumption that an increased brightness/intensity of the filaments translated to higher temperatures was used to determine the electrode geometry of the plasma actuator. Through imaging techniques, it was found that the double saw tooth electrode configuration, with a dielectric barrier and without an interelectrode gap, produced the most well-defined and brightest filaments. However, arcing was a major issue that was faced at high pulse

parameters at atmospheric pressure as well as at lower ambient pressures. Mitigation methods to curb the arcing were studied but none of them were able to entirely solve the problem of arcing.

Temperature measurements of the plasma filaments on the optimized geometry were taken to understand the thermal characteristics of the filaments and how they affected the induced flow. This was done using optical emission spectroscopy and very preliminary values of the rotational and vibrational temperatures were obtained using the software Specair. The inconsistencies in the temperature fits showed that the temperature measurements were much more reliable at a higher pulse repetition frequency, due to the improved signal-to-noise ratio. However, getting the temperature measurements at higher frequencies was hindered by the arcing issue.

Schlieren visualization of the induced flow in quiescent air showed that there was a region of hot gas produced at the near the surface of the electrodes and the pressure waves generated increased with pulse repetition frequency. While imaging of the plasma filaments in supersonic flow showed that Mach 2.0 flow caused the plasma filaments to become much shorter and restricted, schlieren visualization of the shock waves in supersonic flow and the effect of the actuator on the shock waves did not produce accurate images due to the inaccuracies of the ramp model.

Future Work

Future tests will consider using electrodes with better geometrical accuracies and mitigation of localized arcing. By preventing arcing, the plasma filaments can be more efficiently characterized. Fabricating the electrodes and extending the length of the electrodes may be useful in getting rid of the arcing issue. The effect of the length of the electrodes on the filamentary discharges can be investigated. Moreover, pulse energy calculations from voltage and current measurements may be a better way of quantifying the thermal characteristics and finding the optimized electrode

geometry compared to relating the intensity of the filaments to their temperature. More reliable temperature measurements should be taken to further quantify the thermal characteristics. Precision in the alignment of the optics in the optical emission spectroscopy setup and increment of the accumulations of the discharges to get a better experimental spectrum is required to get rotational and vibrational temperatures that are more accurate. Moreover, the temperature at different points on the discharge can be investigated, unlike in this work where the emission from an entire discharge was captured to get the average temperature across it.

There is also a need to investigate the effect of the plasma discharges on the shock wave and shock wave-boundary layer interaction (SWBLI). A ramp model of better geometrical accuracy needs to be built so that unnecessary effects from the model can be avoided when analyzing the interaction between the plasma discharges and the shock waves formed in the flow. The effect of plasma formation direction, i.e. filament growth against vs. with the flow, will also be examined by reversing the placement of the exposed and covered electrodes. The existing schlieren system will be modified to provide high-magnification, high-resolution images of the flat plate boundary layer and/or the SWBLI region. Likely modifications to the schlieren system include implementing a high-power pulsed light source and high-speed camera to provide sufficiently small image exposure time to capture the dynamics of the flow turbulence.

REFERENCES

[1] IATA, "2036 Forecast Reveals Air Passengers Will Nearly Double to 7.8 Billion", International Air Transport Association Press Release No. 55 [online webpage], URL: https://www.iata.org/pressroom/pr/Pages/2017-10-24-01.aspx [cited 12 October 2018].

[2] IPCC, "Summary for Policymakers of IPCC Special Report on Global Warming of 1.5°C approved by governments", Intergovernmental Panel on Climate Change Press Release [online report], URL: https://www.ipcc.ch/pdf/session48/pr_181008_P48_spm_en.pdf [cited 12 October 2018].

[3] Statista, "Total fuel consumption of commercial airlines worldwide between 2005 and 2018 (in billion gallons)", Statista – The Statistics Portal [online statistical data], URL: https://www.statista.com/statistics/655057/fuel-consumption-of-airlines-worldwide/ [cited 12 October 2018].

[4] NASA, "NASA Takes Next Step in Green Aviation X-planes Plans" (2016), NASA Aeronautics Article [online webpage], URL: https://www.nasa.gov/aero/nasa-green-aviation-x-planes [cited 13 October 2018].

[5] NASA, "NASA Armstrong Fact Sheet: NASA X-57 Maxwell" (2018), Nasa Aeronautics Article [online webpage], URL: https://www.nasa.gov/centers/armstrong/news/FactSheets/FS-109.html [cited 13 October 2018].

[6] Erfani, R., Zare-Behtash, H., Hale, C., Kontis, K. (2015). "Development of DBD plasma actuators: The double encapsulated electrode," Acta Astronautica, 109 (2015) 132-143.

[7] Abaas, A., Bugeda, G., Ferrer, E., Fu, Song., Periaux, J., Pons-Prats, J., Valero, E., and Zheng, Y. (2017). "Drag reduction via turbulent boundary layer flow control," Science China, DOI: 10.007/s11431-016-9013-6.

[8] Bieler, H. (2017). "Active flow control concepts and application opportunities," Aircraft Engineering and Aerospace Technology, Vol. 89 Issue: 5, pp. 725-729, DOI: 10.1108/AEAT-01-2017-0015.

[9] Aerospace Research Center, "Aerodynamic Flow Control", The Ohio State University [online webpage], URL: https://arc.osu.edu/research/aerodynamic-flow-control [cited 14 October 2018]

[10] Moghaddam, T., and Neishabouri, N. B. (2017). "On the Active and Passive Flow Separation Control Techniques over Airfoils," ICSMME 2017, IOP Conf. Series: Materials and Science Engineering 248 (2017) 012009, DOI: 10.1088/1757-899X/248/1/012009.

[11] Yousefi, K., Saleh, R., and Zahedi, P. (2014). "Numerical study of blowing and suction slot geometry optimization on NACA 0012 airfoil," Journal of Mechanical Science and Technology, May 2014. DOI: 10.1007/s12206-014-0119-1.

[12] Popkin, S. H., Taylor, T. M., Cybyk, B. Z. (2013). "Development and Application of the SparkJet Actuator for High-Speed Flow Control," John Hopkins APL Technical Digest, Volume 32, Number 1 (2013).

[13] Glezer, A., and Amitay, M. (2002). "Synthetic Jets," Annu. Rev. Fluid Mech. 34(1), 503-529.

[14] Corke, T. C., and Post, M. L. (2005). "Overview of Plasma Flow Control: Concepts, Optimization and Applications," in Proc. 43rd AIAA Aerospace Sciences Meeting and Exhibit, Reno, NV, paper AIAA-2005-563.

[15] Samimy, M., Kastner, J., Kim, H., Utkin, Y., and Adamovich, H. Brown, C. A. (2006). "Flow and Noise Control in High Speed and High Reynolds Number Jets Using Plasma Actuators," The Ohio State University, Columbus, Ohio. Glenn Research Center, Cleveland, Ohio, AIAA-2006-2846.

[16] Samimy, M., Kearney, M. – Fisher, J., Kim, H., and Sinha, A. (2011). "High Speed and High Reynolds Number Jet Control Using Arc Filament Plasma Actuators for Noise Mitigation and for Flow and Noise Diagnostics," 49th AIAA Aerospace Sciences Meeting including the New Horizons Forum and Aerospace Exposition, Orlando, Florida, paper AIAA-2011-22.

[17] Kim, H., Nishihara, M., Adamovich, I.V., and Samimy, M. Gorbatov, S. V., and Pliavaka, F. V. (2010). "Development of Localized Arc Filament RF Plasma Actuators for High-Speed and High Reynolds Number Flow Control," The Ohio State Univerisity, Columbus, Ohio, and A. V. Lykov Heat and Mass Transfer Institute of National Academy of Sciences of Belarus, Minsk, Belarus.

[18] Verma, S. B., Hadjadj, A. (2015). "Supersonic Flow Control," Shock Waves (2015), DOI: 10.1007/s00193-015-0587-y.

[19] Samimy, M., Webb, N., Clifford, C. (2011). "Supersonic Inlet Flow Control Using Localized Arc Filament Plasma Actuators," Gas Dynamics and Turbulence Laboratory, The Ohio State University, Columbus, Ohio. FA9550-09-1-0644.

[20] Syberg, J., Koncsek, J. L. (1976). "Experimental Evaluation of an Analytically Derived Bleed System for a Supersonic Inlet," Journal of Aircraft, Vol. 13, No. 10 (1976), pp. 792-797.

[21] Samimy, M., Kim, J.-H., Kastner, J., Adamovich, I., and Utkin, Y. (2007). "Active control of high-speed and high-Reynolds-number jets using plasma actuators," J. Fluid Mech, Vol. 578, pp. 305-330. DOI: 10.1017/S0022112007004867.

[22] Utkin, Y., Keshav, S., Kim, J.-H., Kastner, J., Adamovich, I., and Samimy, M. (2007). "Development and Use of Localized Arc Filament Plasma Actuators for High-speed Flow Control," J. of Physics D: Applied Physics, 40, 685–694, 2007.

[23] Samimy, M., Worthington, Adamovich, I., Powell. (2008). "Localized Arc Filament Plasma Actuators for Noise Mitigation and Mixing Enhancement," United States Patent, Patent No.: US 7,334,394 B2.

[24] Macheret, S. O., Schneider M. N., Miles, R. B. (2004). "Magnetohydrodynamic and Electrohydrodynamic Control of Hypersonic Flows of Weakly Ionized Plasmas," AIAA Journal, Vol. 42, No. 7, July 2004. DOI: 10.2514/1.3971.

[25] Adamovich, I. V., Leonov, S. B., Frederickson, K., Zheng, J. G., Cui, Y. D., and Khoo, B. C. (2017). "Thermal perturbations generated by near-surface electric discharges and mechanisms of their interaction with the airflow," 55th AIAA Aerospace Sciences Meeting, AIAA SciTech Forum, Grapevine, Texas. DOI: 10.2514/6.2017-1339.

[26] Roupassov, D.V., Nikipelov, A.A., Nudnova, M.M., and Starikovskii, A.Yu., "Flow separation Control Plasma Actuator with Nanosecond Pulsed-Periodic Discharge", AIAA Journal, vol. 47, No. 1, 2009, p.168.

[27] Kim, J.-H., and Samimy, M. (1999). "Mixing enhancements via nozzle trailing edge modifications in a high-speed rectangular jet," Phys. Fluids, DOI: 10.1063/1.870132.

[28] Little, J. (2016). "Thermal Mechanisms for High Amplitude Aerodynamic Flow Control," University of Arizona, Tucson, Arizona. FA9550-12-1-0044.

[29] Samimy, M., Kearney-Fischer, M., Kim, J.-H., and Sinha, A. (2012). "High-Speed and High-Reynolds-Number Jet Control Using Localized Arc Filament Plasma Actuators," Journal of Propulsion and Power, Vol. 28, No. 2, March-April 2012. DOI: 10.2514/1.B34272.

[30] Bogaerts, A., Neyts, E., Gijbels, R., and van der Mullen, J. (2002). "Gas discharge plasmas and their applications," Spectrochim. Acta, Part B 57(4), 609-658. DOI: 10.1016/S0584-8547(01)00406-2.

[31] Loeb, L. B., and Meek, J. M. (1940). "The mechanism of spark discharge in air at atmospheric pressure," J. Appl. Phys., Vol. 11, No. 6, pp. 438-447. DOI: 10.1063/1.1712792.

[32] Samimy, M., Kim, J.-H., Kastner, J., Adamovich, I., and Utkin, Y. (2007). "Active Control of a Mach 0.9 Jet for Noise Mitigation Using Plasma Actuators," AIAA Journal, Vol. 45, No. 4, pp. 890-901.

[33] Leonov, S., Bityurin V., Savelkin, K., Yarantsev, D. (2002). "Effect of electrical discharge on separation processes and shocks position in supersonic airflow," Am Inst Aeronaut Astronaut, Paper 2002-0355.

[34] Leonov, S., Yarantsev, and Sabelnikov, V. (2011). "Electrically driven combustion near the plane wall in a supersonic duct," Prog. Propul. Phys., Vol. 2, pp. 519-530. DOI: 10.1051/eucass/201102519.

[35] Leonov, S., Bityurin, V., Savelkin, K., and Yarantsev, D. (2003). "Progress in investigation for plasma control of duct-driven flows," 41st Aerospace Sciences Meeting and Exhibit, AIAA, Reno, Vol. 699.

[36] Bianchi, G., Saracoglu, B. H., Paniagua, G., and Regert, T. (2015). "Experimental Analysis on the Effects of DC Arc Discharges at Various Flow Regimes," Physics of Fluids, Vol. 27, p. 03612.

[37] Wang, J., Li, Y. H., and Xing, F. (2009). "Investigation on oblique shock wave control by arc discharge plasma in supersonic flow," Journal of Applied Physics 106, 073307. DOI: 10.1063/1.3236658.

[38] Sun, Q., et al. (2014). "The characteristics of surface arc plasma and its control effect on supersonic flow," Physics Letter A, Vol. 378, Issue 36, pp. 2672-2682.

[39] Sun, Q., et al. (2013). "Computational and experimental analysis of Mach 2 air flow over a blunt body with plasma actuation," Science China-Technological Sciences, Vol. 56, Issue 4, pp. 795-802.

[40] Sun, Q., et al. (2013). "Experimental Investigation on Airfoil Shock Control by Plasma Aerodynamic Actuation," Plasma Science & Technology, Vol. 15, Issue 11, pp. 1136-1143.

[41] Adamovich, I., Little, J., Nishihara, M., Takashima, K., Samimy, M. (2012). "Nanosecond pulse surface discharges for high-speed flow control", AIAA Paper 2012-3137, 6th AIAA Flow Control Conference, New Orleans, Louisiana, 25-28 June.

[42] Moreau, E. (2007). "Airflow control by non-thermal plasma actuators," Journal of Physics D: Applied Physics, Volume 40, No.3.

[43] Nishihara, M., Takashima, K., Rich J. W., and Adamovich, I.V. (2011). "Mach 5 Bow Shock Control by a Nanosecond Pulse Surface Dielectric Barrier Discharge," Physics of Fluids, Vol. 23, p. 066101.

[44] Nishihara, M., Gaitonde, D., and Adamovich, I. V. (2013) "Effect of Nanosecond Pulse Discharges on Oblique Shock and Shock Wave-Boundary Layer Interaction," AIAA Paper 2013-0461, 51st AIAA Aerospace Sciences Meeting, Grapevine, Texas, 7-10 January.

[45] Kinefuchi, K., Starikovskiy, A.Y., and Miles, R.B. (2016) "Control of shock wave-boundary layer interaction using nanosecond dielectric barrier discharge plasma actuators", AIAA Paper 2016-5070, 52nd AIAA/SAE/ASEE Joint Propulsion Conference, Salt Lake City, UT.

[46] Yang, D., Wang, W., Jia, L., Nie, D., and Shi, H. (2011). "Production of atmospheric pressure diffuse nanosecond pulsed dielectric barrier discharge using the array needles-plate electrode in air", Journal of Applied Physics 109, 073308.

[47] Opaits, D.F., et al. (2008). "Experimental investigation of dielectric barrier discharge plasma actuators driven by repetitive high-voltage nanosecond pulses with dc or low frequency sinusoidal bias", Journal of Applied Physics 104, 043304.

[48] Gibalov, V., and Pietsch, G. (2000). "The development of dielectric barrier discharges in gas gaps and on surfaces", J. Phys. D: Appl. Phys, Volume 33, 2618-2636.

[49] Starikovskii, A., Nikipelov, A., Nudnova, M., and Roupassov, D. (2009). "SDBD plasma actuator with nanosecond pulse-periodic discharge", Plasma Sources Science and Technology, Volume 18, 034015.

[50] Newnam, K. (2017). "Characterization of Plasma Formation and Induced Flows of Nanosecond-Pulsed Dielectric Barrier Discharges for Use in Supersonic Flow Control," M.S. Thesis, Department of Aeronautical and Astronautical Engineering, Purdue University, West Lafayette, IN.

[51] Wang, C.C., and Roy, S. (2012). "Energy and force prediction for a nanosecond pulsed dielectric barrier discharge actuator", Journal of Applied Physics 111, 103302.

[52] Song, H., Zhang, Q., Li, Y., Jia, M., Wu, Y., and Liang H. (20120. "Plasma Sheet Actuator Driven Repetitive Nanosecond Pulses with a Negative DC Component", Plasma Science and Technology, Vol. 14, No.4, Apr.

[53] Tirumala, R., Bernard, N., Moreau, E., Fenot, M., Lalizel, G., and Dorignac, E. (2014). "Temperature characterization of dielectric barrier discharge actuators: influence of electrical and geometrical parameters," Journal of Physics D: Applied Physics, Vol. 47 (255203), pp. 1-12.

[54] Joussot, R. et al. (2010). "Thermal Characterization of a DBD Plasma Actuator: Dielectric Temperature Measurements using Infrared Thermography," 40th Fluid Dynamics Conference and Exhibit, AIAA 2010-5102, Chicago, Illinois, 28 June-1 July.

[55] Jukes, T. N., Choi, K. Johnson, G. A., and Scott, S. J. (2006). "Characterization of a surface-induced wall flows through velocity and temperature measurements," AIAA Journal, Vol. 44, pp. 764-771.

[56] Jukes, T. N., Choi, K., Segawa, T., and Yoshida, H. (2008). "Jet flow induced by a surface plasma actuator," Proc. Inst. Mech. Eng., Vol. 222, pp. 347-356.

[57] Dong, B., Bauchire, J. M., Pouvesle, J. M., Magnier, P., and Hong, D. (2008). "Experimental study of a dbd surface discharge for the active control of subsonic airflow," Journal of Physics D: Applied Physics, Volume 41 (155201), pp. 1-9.

[58] Stanfield, S. A., Menart, J., DeJoseph, C., Kimmel, R. L., and Hayes, J. R. (2009). "Rotational and vibrational temperature distributions for a dielectric barrier discharge in air," AIAA Journal, Vol. 47, No. 5, pp. 1107-1115.

[59] Little, J., Takashima, K., Nishihara, M., Adamovich, I., and Samimy, M. (2012). "Separation control with nanosecond-pulse-driven dielectric barrier discharge plasma actuators," AIAA Journal, Vol. 50, pp. 350-365.

[60] Correale G., Michelis, T., Ragni, D., Kotsonis, M., and Scarano, F. (2014). "Nanosecond-pulsed plasma actuation in quiescent air and laminar boundary layer," Journal of Physics D: Applied Physics, Volume 47 (105201).

[61] Starikovskii, A. Y., Nikipelov, A. A., Nudnova, M. M., and Roupassov, D. V. (2009). "Sdbd plasma actuator with nanosecond pulse-periodic discharge," Plasma Sources Sci. Technol. Volume 18. 034015.

[62] Takashima, K., Zuzeek, Y., Lempert, W. R., and Adamovich, I. V. (2011). "Characterization of a surface dielectric barrier discharge plasma sustained by repetitive nanosecond pulses," Plasma Sources Sci. Technol. Volume 20. 055009.

[63] Cui, Y. D., Zhao, Z. J., Bouremel, Y., Li, J., Zheng, J. G., Hu, F. G., and Khoo, B. C. (2014). "Studies on the Configurations of Nanosecond DBD Pulse Plasma Actuators," 19th Australian Fluid Mechanics Conference, Melbourne, 8-11 December.

[64] Thomas, F. O., Corke, T. C., Iqbal, M., Kozlov, A., and Schatzman, D. (2009). "Optimization of Dielectric Barrier Discharge Plasma Actuators for Active Aerodynamic Flow Control," AIAA Journal, Vol. 47, No. 9, DOI: 10.2514/1.41588.

[65] Bayoda, K. D., Benard, N., and Moreau, E. (2015). "Electrical and mechanical characteristics of nanosecond pulsed sliding dielectric barrier discharges with different electrode gaps," Journal of Physics Conference Series, November. DOI: 10.1088/1742-6596/646/1/012054.

[66] Ndong, A. C., Zouzou, N., Benard, N., and Moreau, E. (2013). "Geometrical optimization of a surface DBD powered by a nanosecond pulsed high voltage," Journal of Electrostatics, **71**, pp. 246-253.

[67] Dawson, R. A., and Little, J. (2013). "Effects of pulse polarity on nanosecond pulse driven dielectric barrier discharge plasma actuators," 43rd Fluid Dynamics Conference, June 24-27, San Diego, CA.

[68] Wu, Y., Li, Y., Jia, M., Song, H., Guo, Z., Zhu, X., and Pu, Y. (2008). "Influence of operating pressure on surface dielectric barrier discharge plasma aerodynamic actuation characteristics," Appl. Phys. Lett. **93**, 031503. https://doi.org/10.1063/1.2964193.

[69] Nichols, T. G., and Rovey, J. L. (2012). "Fundamental Processes of DBD Plasma Actuators Operating at High Altitude," 50th AIAA Aerospace Sciences Meeting, 9-12 January, Nashville, Tennessee, AIAA 2012-0822.

[70] Rodrigues, F. F., Pascoa, J. C., and Trancossi, M. (2018). "Experimental Analysis of Alternative Dielectric Materials for DBD Plasma Actuator," Proceedings of the ASME 2018 International Mechanical Engineering Congress and Exposition (IMECE), Pittsburgh, PA, November 9-15. IMECE2018-87455.

[71] Correale, G., Winkel, R., and Kotsonis, M. (2015). "Energy deposition characteristics of nanosecond dielectric barrier discharge plasma actuators: Influence of dielectric material," Journal of Applied Physics, **118**, 083301. http://dx.doi.org/10.1063/1.4929362.

[72] Rodrigues, F., Pascoa, J., and Trancossi, M. (2018). "Heat generation mechanisms of dbd plasma actuators," Experimental Thermal and Fluid Science, **90**, pp. 55-65.

[73] Houser, N. M., Gimeno, L., Hanson, R. E., Goldhawk, T., Simpson, T., and Lavoie, P. (2013). "Microfabrication of dielectric barrier discharge plasma actuators for flow control," ScienceDirect, Sensors and Actuators A: Physical, Volume 201, https://doi.org/10.1016/j.sna.2013.06.005.

[74] Ndong, A., Zouzou, N., Benard, N., and Moreau, E. (2013). "Effect of the dielectric aging on the behavior of a surface nanosecond pulsed DBD," ResearchGate, IEEE Transactions on Dielectrics and Electrical Insulation, DOI: 10.1109/TDEI.2013.6633683.

[75] Hanson, R. E., Houser, N. M., and Lavoie, P. (2014). "Dielectric material degradation monitoring of dielectric barrier discharge plasma actuators," Journal of Applied Physics, **115**(043301), pp. 1-9.

[76] Chatelain, K., Joussot, R., Leroy, A., Lago, V., Rabat, H., and Hong, D. (2014). "Discharge morphology and spectral diagnostic of a serrated dbd plasma actuator dedicated to aerodynamic flow control applications," Univ. Orleans, France.